UNIVERSITY OF OKLAHOMA

GRADUATE COLLEGE

MEASUREMENT AND 3D FINITE ELEMENT MODELING OF BLAST WAVE TRANSMISSION THROUGH CHINCHILLA EAR

A THESIS

SUBMITTED TO THE GRADUATE FACULTY

in partial fulfillment of the requirements for the

Degree of

MASTER OF SCIENCE

By

PAIGE WELCH
Norman, Oklahoma
2020

MEASUREMENT AND 3D FINITE ELEMENT MODELING OF BLAST WAVE TRANSMISSION THROUGH CHINCHILLA EAR

A THESIS APPROVED FOR THE
STEPHENSON SCHOOL OF BIOMEDICAL ENGINEERING

BY THE COMMITTEE CONSISTING OF

Dr. Rong Gan, Chair

Dr. Vassilios Sikavitsas

Dr. Chenkai Dai

Acknowledgements

I would like to thank everyone in lab who has helped me in my research progress. First and foremost, I would like to thank my advisor, Dr. Rong Gan, for her guidance and advice during my time in her lab. Her mentorship in my research career has been invaluable. I would like to thank Shangyuan Jiang for his assistance in animal studies. I am also thankful for the help Marcus Brown provided in computer modeling. I would also like to thank Kyle Smith for his part in the animal studies and computer modeling. I am so thankful for all of their collegiality over these past few years. In addition, I am tremendously grateful to Dr. Xuelin Wang for his Finite Element Analysis expertise and for assisting in modifying the mesh of the FE model of the chinchilla ear.

I would also like to thank Dr. Alisha Preno and the veterinary staff for their hard work with taking care of the animals. They played a critical role that allowed studies to run smoothly and I appreciate their exemplary performance.

Furthermore, I would like to thank the Stephenson School of Biomedical Engineering for sponsoring my teaching assistantship and for funding my trip to the Biomedical Engineering Society Annual Meeting 2019.

This work would not be possible without the support of the Department of Defense grants W81XWH-14-1-0228 and W81XWH-19-1-0469.

Finally, I am incredibly thankful for the love and support that my family has given me my whole life.

Table of Contents

Acknowledgements iv

List of Tables viii

List of Figures ix

Abstract xiv

Chapter 1: Introduction 1

1.1 Motivation 1

1.2 The Auditory System 2

1.2.1 The Peripheral Auditory System (PAS) 2

1.2.2 The Central Auditory System (CAS) 4

1.3 Blast-Induced Hearing Loss in Animal Models 5

1.4 Finite Element Models for Blast Wave Transmission in the Ear 7

1.4.1 FE Model of the Human Ear 7

1.4.2 FE Model of the Chinchilla Middle Ear 9

1.5 Objectives 11

Chapter 2: Auditory Dysfunction Induced by Repeated Low Intensity Blast Exposures in a Chinchilla Model 12

2.1 Animal Model – Chinchilla 12

2.2 Experimental Design 13

2.3 Hearing Function Tests 16

2.3.1 Auditory Brainstem Response (ABR) 16

2.3.2 Distortion Product Otoacoustic Emissions (DPOAE) 17

2.3.3. Middle Latency Responses (MLR) 17

2.4 Statistical Analysis 18
2.5 Results 18
2.5.1 BOP Waveforms 18
2.5.2 ABR Threshold Shifts 19
2.5.3 ABR Wave I Amplitudes 22
2.5.4 DPOAE Level Shifts 23
2.5.5 Assessment of Central Auditory System Damage (MLRs) 24
2.5.6 Discussion 27
2.5.6.1 Hearing Damage Induced by Repeated Low-Intensity BOPs 27
2.5.6.2 Effect of Number of Blasts and HPDs 28
2.6 Chapter Summary 31
Chapter 3: 3D FE Model of Chinchilla Ear for Acoustic Sound Transmission 33
3.1 Creation of 3D FE Model of Chinchilla Ear 33
3.1.1 3D FE Model of the Chinchilla Middle Ear 33
3.1.2 Chinchilla Cochlea Model 35
3.1.3 Creation of 3D FE Model of Chinchilla Ear 38
3.2 Generating Model for Harmonic Response Analysis 40
3.2.1 ANSYS Workbench 41
3.2.2 Structural Analysis in ANSYS Mechanical: Harmonic Response 41
3.2.3 Equations Governing Acoustic Elements 42
3.2.4 ANSYS Harmonic Response Analysis Setup 43
3.3 Results and Validation 45
3.4 Chapter Summary 51

Chapter 4: 3D FE Model of Chinchilla Ear for Blast Wave Transmission 53
4.1 Strongly Coupled FSI Analysis Scheme for Modeling Blast Wave Transmission 53
4.2 Generating Model for Blast Wave Simulation..... 56
4.2.1 Fluid Analysis Setup 56
4.2.2 ANSYS Mechanical Analysis Setup..... 60
4.3 Results..... 62
4.3.1 Discussion 68
4.4 Chapter Summary 70
Chapter 5: Conclusion..... 72
5.1 Research Summary 72
5.2 Future Work..... 73
References..... 75
Appendix A: List of Abbreviations..... 82

List of Tables

Table 1: Material properties of chinchilla ear model for blast wave analysis 61

List of Figures

Figure 1. Anatomy of the human ear. (https://www.hearinglink.org/your-hearing/about-hearing/how-the-ear-works/)..... 3

Figure 2. Cross-section of the cochlea with enlarged organ of Corti. (https://www.researchgate.net/figure/Cross-section-of-the-cochlea-with-enlarged-organ-of-Corti-40_fig1_330111901)..... 4

Figure 3. Schematic diagram of the auditory pathway from the cochlea, including auditory structures within the brainstem (1), midbrain (2), and cortex (3).(Hall, 2012). . 5

Figure 4. FE model of the human ear used to simulate blast wave transmission. (Leckness et al., 2018). 9

Figure 5. 3D FE model of the chinchilla ear developed by Wang & Gan (2016). 10

Figure 6. Timeline of experimental procedures.. 13

Figure 7. Schematic of animal experimental setup with blast apparatus. 15

Figure 8. A recorded BOP waveform at the entrance of the ear canal from an animal test with earplugs with a peak pressure of 4.0 psi. 19

Figure 9. (A) ABR threshold shifts (mean ± SEM, n = 14) measured in plugged ears after 6 blasts on Day 1, Day 4, and Day 14. (B) ABR threshold shifts (mean ± SEM, n = 14) measured in open ears after 6 blasts on Day 1, Day 4, and Day 14. (C) Comparison of ABR threshold shifts in plugged and open ears on Days 1, 4, and 14. 21

Figure 10. ABR wave I amplitude in response to stimulus level from 40 to 100 dB SPL measured from (top) open ears (mean ± SEM, n = 14) and (bottom) plugged ears (mean ± SEM, n = 14). 23

Figure 11. DPOAE level shifts (mean ± SEM, n = 14) measured from protected ears on Days 1 and 14.....24
Figure 12. Representative MLR traces from chinchilla with unprotected ears taken (A) pre-blast (B) post-blast and (C) Day 14.. 25
Figure 13. MLR results at 80 dB SPL in open and protected ears after exposure to 6 consecutive low-intensity blasts of 21-35 kPa (3-5 psi).. 27
Figure 14. ABR threshold shifts (mean ± SEM) measured in open ears on Days 1, 4, and 7 after exposure to low-intensity blasts of 21-35 kPa (3-5 psi). (A) 6 consecutive blasts (n=14) and (B) 3 consecutive blasts (n=7) (Fig.5B, Chen, 2019). 29
Figure 15. ABR threshold shifts (mean ± SEM) measured in protected ears on Days 1, 4, and 7 after exposure to low-intensity blasts of 21-35 kPa (3-5 psi). (A) 6 consecutive blasts (n=14) and (B) 3 consecutive blasts (n=7) (Fig.5A, Chen, 2019). 29
Figure 16. ABR wave I amplitude (mean ± SEM) in response to stimulus level from 80 to 100 dB SPL measured from (A-B) open ears and (C-D) protected ears after exposure to low-intensity blasts of 21-35 kPa (3-5 psi). (A, C) 6 consecutive blasts (n=14) and (B, D) 3 consecutive blasts (n=7) (Fig.6, Chen, 2019). 30
Figure 17. DPOAE level shifts (mean ± SEM) measured from protected ears on Days 1, 4, and 7 after exposure to (A) 6 consecutive blasts (n=14) and (B) 3 consecutive blasts (n=7) (Fig.7A, Chen, 2019). 31
Figure 18. (A) A typical μCT image of a chinchilla left ear with (B) bony structure outlined in blue (Wang & Gan, 2016).. 34
Figure 19. 3D FE model of the chinchilla middle ear (Wang & Gan, 2016).....35

Figure 20. FE model the chinchilla cochlea with middle ear components (stapes, stapedial annular ligament, and round window membrane) to illustrate connection points to the middle ear model. 36
Figure 21. Basilar membrane structure and associated bony supports of the FE model of the chinchilla cochlea. 37
Figure 22. Basilar membrane and associated bony supports surrounded by cochlear fluid (transparent). 37
Figure 23. Posterior view of the 3D FE model of the chinchilla ear including the external ear canal. 38
Figure 24. Medial view of the FE model of the chinchilla ear including the ear canal, TM, ossicular chain and supporting ligaments, septa, and cochlea. 39
Figure 25. Posterior view of the middle ear structures and cochlea. The connection between the TM and cochlea through the ossicular chain is prominently displayed. Note the emphasis on suspensory ligaments.. 39
Figure 26. Young's modulus gradient from base to apex 44
Figure 27. β damping coefficient gradient from base to apex. 44
Figure 28. FE model derived displacements of the (A) TM at the umbo and (B) stapes FP in comparison to the published FE model of the chinchilla middle ear (Wang & Gan, 2016). 46
Figure 29. FE model-derived displacements of the (A) TM at the umbo and (B) stapes FP in comparison to published experimental data in chinchilla (Guan et al., 2014; Ruggero et al., 1990). 47

Figure 30. BM displacement normalized with respect to the footplate displacement (d_{BM} / d_{FP}) at frequencies of 200 Hz – 15 kHz from the base to apex. 48
Figure 31. FE model-derived frequency versus position map in comparison to published chinchilla experimental data. The black line represents the line of best fit to data points (Eldredge et al., 1981). 49
Figure 32. ANSYS Workbench project schematic showing data flow from FLUENT and ANSYS Mechanical (Transient Structural) to system coupling. 55
Figure 33. (A) A recorded BOP waveform at the entrance of the ear canal from an animal test with a peak pressure of 4.7 psi. (B) Model image with the entrance of the ear canal in light blue.. 57
Figure 34. P0, P1, and P2 pressure monitors in the ear canal and middle ear cavity. 59
Figure 35. Locations of the pressure monitors in the scala vestibuli (SV-1, SV-2, and SV-3) and scala tympani (ST-1, ST-2, and ST-3) 60
Figure 36. Representative waveforms recorded at the entrance of the ear canal (P0) and near the TM in the canal (P1) from chinchilla animal model used in blast exposure study (Chen et al., 2019). 63
Figure 37. FE model-predicted pressure waveforms at the entrance of the ear canal (P0), in front of the TM in the canal (P1), and behind the TM in the middle ear cavity (P2).. 64
Figure 38. FE model-derived pressures in the cochlea in response to BOP input. Pressure was calculated at three different points in the scala vestibuli (SV) and scala tympani (ST) each.. 65
Figure 39. Model-predicted displacements of the (A) TM at the umbo and (B) stapes footplate in the normal direction in response to BOP input. 66

Figure 40. Basilar membrane displacement from base to apex in response to BOP in the time domain. 67

Abstract

Hearing loss caused by blast exposure is an inherent risk that active Service members face due to the operational activities they engage in. With auditory system dysfunction dominating service-connected disabilities among Veterans, there is an urgent need to better understand the effects of blast exposure on the auditory system, particularly the effects of repeated low-intensity blast exposure on progressive hearing loss. Furthermore, the analysis of blast wave transmission in the ear is needed.

This thesis focuses on an experimental study using chinchilla animal model. Chinchilla with and without earplugs were exposed to repeated low-intensity blasts. Hearing function tests reflecting the state of the auditory system were measured prior to blast, after blast, and were then monitored over 14 days.

This thesis also reports the creation of the first finite element model of the entire chinchilla ear, including spiral cochlea. A finite element (FE) model of the chinchilla cochlea was integrated with our lab's previously published FE model of the chinchilla middle ear. The model was first evaluated for simulating acoustic sound transmission. A uniform acoustic pressure applied as an input and harmonic response analysis was conducted. The model was then validated by comparing model-predicted movements of ear structures with experimental measurements.

The FE model of the entire chinchilla ear was then adapted for blast wave analysis. Pressure waveforms measured during chinchilla blast exposure studies were applied to the model as input. The model-predicted waveforms at locations within the ear were then compared with experimental waveforms recorded in the same locations. Movement of structures within the ear were also predicted.

The work presented in this thesis improves our understanding of the effects of blast exposure on the auditory system. Experimental data collected from chinchilla animal model provides insight into the effect of low-intensity blasts on hearing damage, which is not well studied. Moreover, this study provides information on the central auditory system, which is lacking in the literature. Furthermore, this thesis reports the first FE model of the entire chinchilla ear. This model provides a computational tool to simulate the sound or blast wave transmission through the chinchilla ear, explain experimental observations in animal model of chinchilla, and help translate animal experimental data to human responses to blast exposure. Future work includes further investigation of different blast conditions (e.g. number of blasts, blast intensity, recovery time, etc.) on hearing loss and improvement of the FE model for blast wave analysis.

Chapter 1: Introduction

1.1 Motivation

Auditory system disabilities greatly affect Service members and Veterans. Tinnitus and hearing loss are the two most prevalent service-connected (SC) disabilities overall among Veterans (Benefits Administration - The Office of Performance Analysis, 2019).These disabilities not only impose a large economic expense on the part of the Veterans Health Administration, with approximately 3.2 million Veterans receiving SC auditory disability compensation in FY 2018 (Benefits Administration - The Office of Performance Analysis, 2019), but they also affect the quality of life of those who are disabled.

Hearing damage caused by blast waves is an inherent risk among military Service members due to the operational activities they perform. Blast overpressure (BOP) is a high intensity disturbance in the ambient air pressure (Stuhmiller et al., 1991). In the military, BOP exposure typically occurs from muzzle blast from firing heavy weapons and upon detonation of explosives and munitions as in incoming artillery rounds (Patterson & Hamernik, 1997). Blast pressure waves exert forces primarily at air-tissue interfaces within the body, placing the auditory system at high risk of damage.

Animal models such as chinchilla have been established to investigate the effect of BOP exposure on hearing loss. However, most studies have focused on high-level BOP exposure, though evidence has shown that low-level BOPs may also induce hearing damage. Furthermore, few studies have assessed the effect of exposure to repeated blasts, which reflects the reality of Service members in combat or in training drills. To provide a

more comprehensive understanding of blast-induced hearing damage, these underrepresented circumstances should be investigated.

Finite element (FE) models have been established to buttress experimental animal models, serving to link the structure of the ear and its function. While a model that predicts the human ear response to pressure waveforms has been developed, no such model exists for the chinchilla ear. To improve our understanding of the mechanisms of blast-induced hearing loss, a model that can predict the response of the chinchilla ear to BOP waveforms must be developed.

1.2 The Auditory System

The auditory system is categorized into two parts: the peripheral auditory system (PAS) and central auditory system (CAS). This section will provide a brief overview of each, including relevant structures and functions.

1.2.1 The Peripheral Auditory System (PAS)

The PAS consists of the ear, which may be broken down into three sections: the outer ear, middle ear, and inner ear. The outer ear consists of the pinna (the structure that we visually recognize as the ear) and the external ear canal, which ends at the tympanic membrane (TM) or eardrum. The main function of the outer ear is to collect and funnel sound waves towards the TM. The middle ear consists of the TM, which is connected by the manubrium to the ossicles. The ossicular chain itself is composed of the malleus, incus, and stapes, and terminates at the oval window of the cochlea or inner ear. These middle ear structures are held in place by several suspensory ligaments. When the sound waves meet

the TM, the TM vibrations cause the ossicles to move. The ossicles, which may be thought of as a compound lever, are able to amplify these vibrations and transmit them to the cochlea through the piston-like motion of the stapes. The cochlea or inner ear is filled with fluid and contains the organ of Corti, which is composed of the basilar membrane, upon which mechanosensory hair cells reside (**Figure 2**). The piston-like motion of the stapes causes the fluid in the cochlea to move, exciting the hair cells in the organ of Corti, which produces electrical signals that are then processed by the brain. The anatomy of the human ear is shown in **Figure 1** in a schematic diagram.

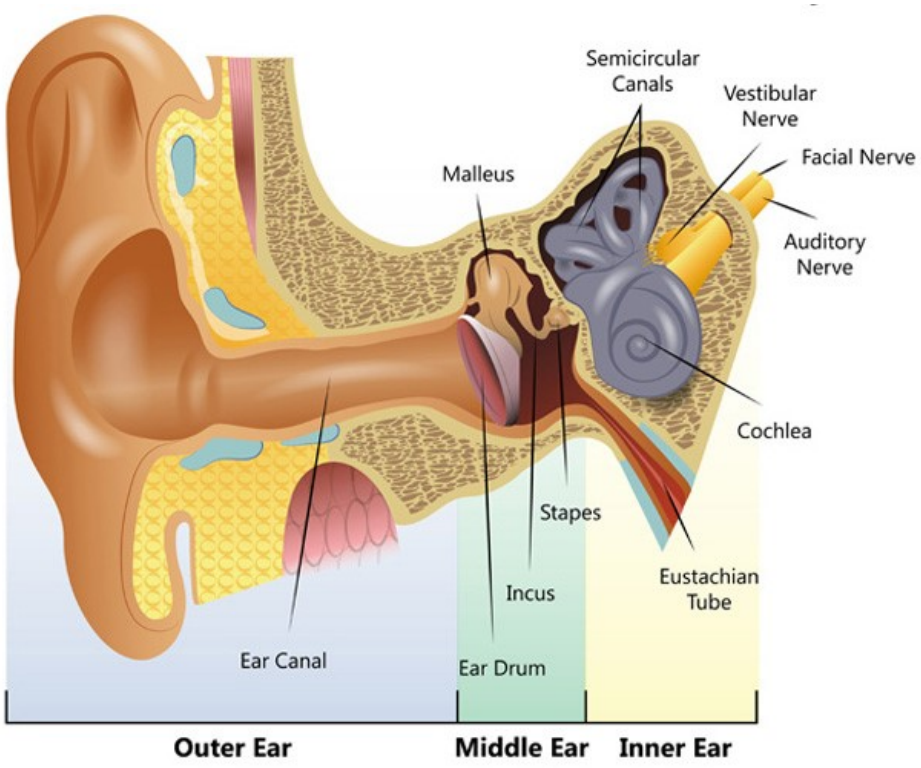

Figure 1. Anatomy of the human ear. The outer ear, middle ear, and inner ear segments and their respective structures are labeled. (https://www.hearinglink.org/your-hearing/about-hearing/how-the-ear-works/)

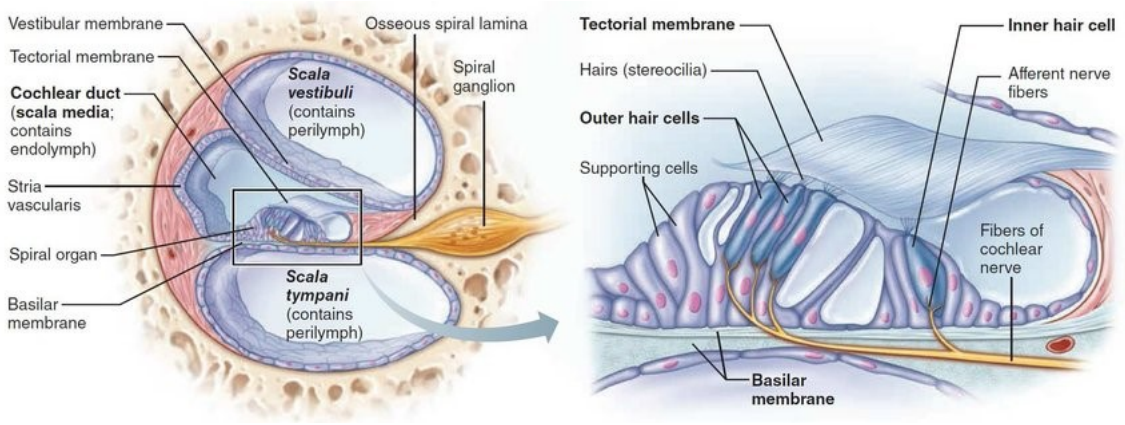

Figure 2. Cross-section of the cochlea with enlarged organ of Corti. Electrical signals are created in the cochlea due to the interaction of the basilar membrane, hair cells and associated stereocilia, and tectorial membrane. Note that the basilar membrane is found above the scala tympani. (https://www.researchgate.net/figure/Cross-section-of-the-cochlea-with-enlarged-organ-of-Corti-40_fig1_330111901)

1.2.2 The Central Auditory System (CAS)

The structures and processes discussed thus far belong to PAS. The electrical signals that result from the excitation of hair cells in the organ of Corti exit the PAS via the cochlear nerve to the (CAS), which includes the auditory pathway from the cochlear nucleus up to the primary auditory cortex. The CAS is responsible for processing and interpreting the auditory information from the cochlea. A schematic diagram of the auditory pathway from the cochlea to the auditory cortex is shown in **Figure 3**.

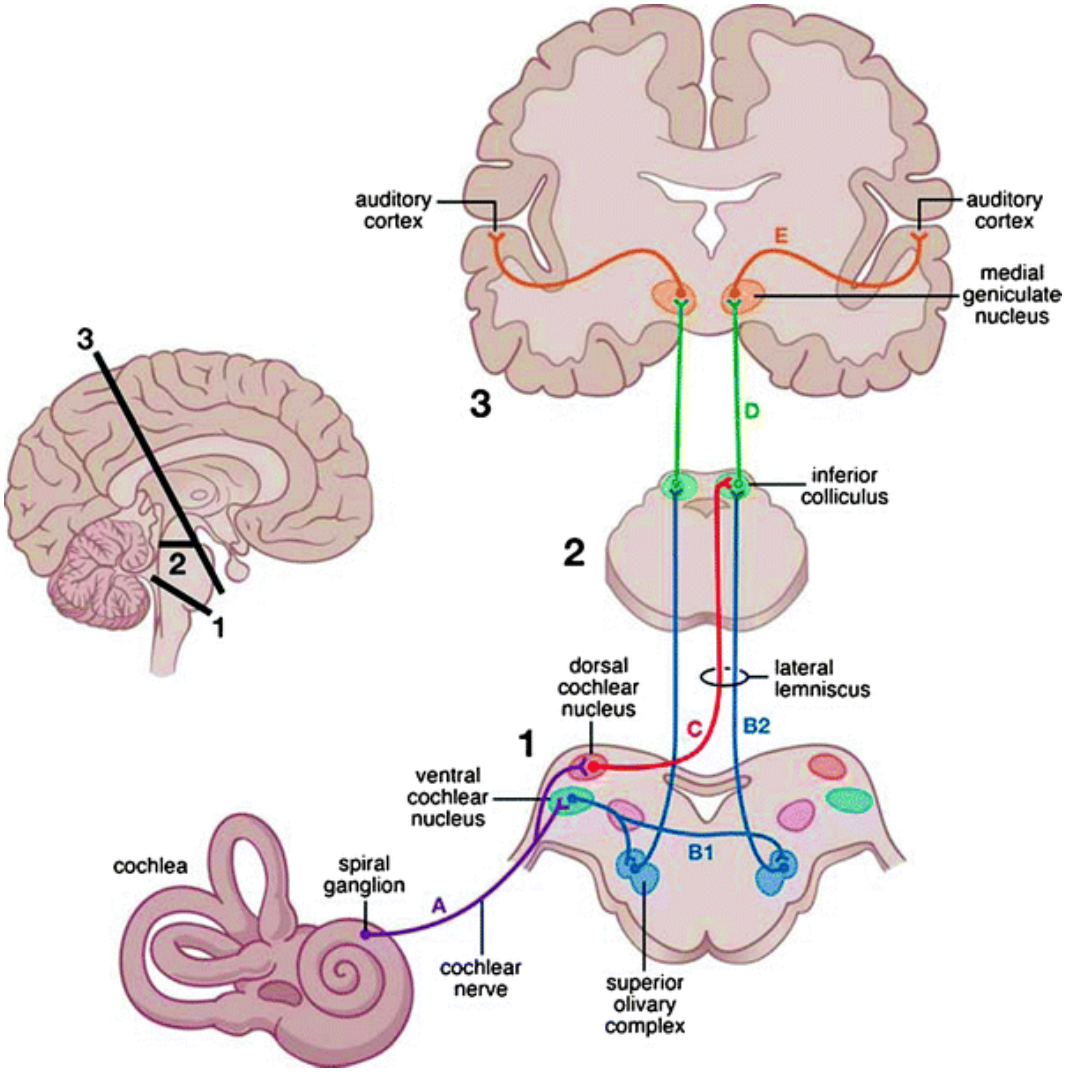

Figure 3. Schematic diagram of the auditory pathway from the cochlea, including auditory structures within the brainstem (1), midbrain (2), and cortex (3). Auditory information from the cochlear is transmitted to the cochlear nucleus via the cochlear nerve (A). Further processing occurs in an ascending auditory pathway: ventral cochlear nucleus to superior olivary complex (B1), superior olivary complex to inferior colliculus (B2), dorsal cochlear nucleus to inferior colliculus (C) inferior colliculus to medial geniculate nucleus (D), and medial geniculate nucleus to auditory cortex (E) (Hall, 2012).

1.3 Blast-Induced Hearing Loss in Animal Models

A variety of animal models, including rat, guinea pig, non-human primate, and chinchilla, have been used to study blast-induced hearing loss (Le Prell et al., 2019). Literature has shown that BOP induces damage to both the PAS and CAS. Studies in

chinchilla and pig animal models, as well as human case studies, have demonstrated that exposure to BOP can result in the rupture of the TM and fracture or dislocate the middle ear ossicles, resulting in conductive hearing loss (Gan et al., 2016; Hirsch, 1968; Patterson & Hamernik, 1997). Sensorineural hearing loss, or hearing loss associated with damage to the inner ear, may also result from blast exposure. Cho et al. (2013) reported significant loss of hair cells and spiral ganglion neurons in mice after exposure to high-intensity blast (186 kPa) (Cho et al., 2013). Excitotoxicity of the spiral ganglion neurons disrupts the synaptic communication between the hair cells and cochlear nerve fibers, leading to auditory dysfunction (Liberman & Kujawa, 2017). The CAS is also vulnerable to blast. Blast waves travel through the air and pass through the skull, transferring kinetic energy from the blast into the brain. This causes a sudden change in intracranial pressure, resulting in shearing and stretching forces that damage regions such as the brainstem and auditory cortex (Fausti et al., 2009). Even low-intensity blast exposure has been shown to induce ultrastructural brain abnormalities (Song et al., 2018).

Recently, Smith et al. (2020) studied the effects of repeated exposure to high-intensity BOP (15-20 psi) on hearing damage in chinchillas. This study demonstrated that ears with hearing protection devices (HPDS, e.g. earplugs) could recover from 2 high-intensity blasts after 7 days. However, 3 blasts under the same conditions resulted in hearing loss that had not recovered after 14 days (Smith et al., 2020). In a similar study, Chen et al. (2019) investigated the effects of repeated exposure to low-intensity BOP (3-5 psi) on hearing damage in chinchillas. This study found that 3 repeated blasts caused temporary damage in protected ears, but permanent hearing impairment in unprotected ears remained 7 days post-blast (Chen et al., 2019). However, the hearing damage caused by

low BOP in relation to the number of blasts (e.g. more than 3 blasts) and the post-blast recovery time (e.g. more than 7 days) is unclear. Moreover, most studies have focused on the effects of exposure to moderate to high BOP levels (DeKosky et al., 2010; DePalma & Hoffman, 2018; Song et al., 2018), while few animal studies have investigated outcomes from low-level blasts. In addition, the protection mechanism of HPDs to the CAS injury during blast exposure needs further studies.

In this thesis, progressive hearing damage after exposure to 6 repeated low-intensity (3-5 psi or 21-35 kPa) blasts and the protective mechanism of earplugs was investigated.

1.4 Finite Element Models for Blast Wave Transmission in the Ear

The finite element method (FEM) is a powerful method for solving problems of engineering models. Complex geometries are discretized into smaller, simpler parts known as finite elements, which are governed by equations that simulate engineering phenomena. Of interest to this thesis are finite element models that have been developed for blast wave analysis in the ear.

1.4.1 FE Model of the Human Ear

In 2004, the Biomedical Engineering Laboratory at the University of Oklahoma, Norman, constructed a FE model of the human ear based on histological section images of a left ear temporal bone. This model was validated by comparing experimental measurements of the stapes footplate (FP) and TM displacements and model-predicted displacements of the two structures. This was the first FE analysis to use acoustic-structure coupled behavior (Gan et al., 2004). The model originally included the fluid domains of

the ear canal and middle ear cavity, TM and TM annulus, the middle ear ossicles and associate suspensory ligaments, and a mass block and dashpot to simulate the cochlear load at the stapes FP. This model evolved to include hyperelastic materials and a simplified two-chamber straight cochlea with the basilar membrane, which was used to predict sound transmission from the ear canal into the cochlea (Gan et al., 2007). Since its creation, the FE model of the human ear has been used to predict middle ear function after TM perforation (Gan et al., 2009) simulate ear damage and disease (Zhang & Gan, 2013), and evaluate a totally implantable hearing systems (Gan et al., 2010).

Recently, Leckness et al. (2018) reported the adaptation of this model to simulate blast wave transmission through the ear. Blast pressure waveforms recorded external to the ear in human cadaver temporal bone studies were applied as an input pressure (P0) at the entrance of the ear canal in the model. The pressure waveforms in front of the TM in the ear canal (P1) and behind the TM in the middle ear cavity (P2) were calculated. The model used and location of the pressure monitors in the model are shown in **Figure 4.** The model was validated by comparing the predicted pressure waveforms and experimentally recorded waveforms, which were found to be in close agreement (Leckness et al., 2018). The model was further validated by comparing model-derived TM displacement under BOP and experimental measurements of the TM under BOP (Jiang et al., 2019). A current limitation of this model is that the cochlea is simplified using a mass block dashpot.

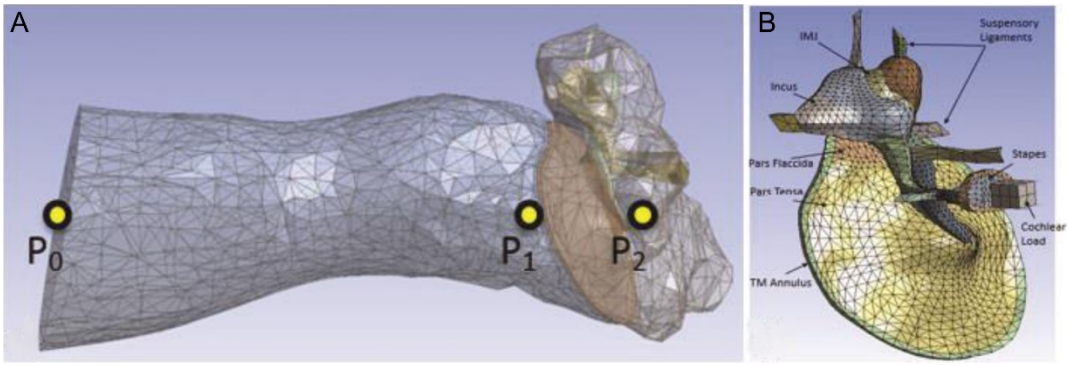

Figure 4. FE model of the human ear used to simulate blast wave transmission. (A) Shows the pressure monitor locations P0, P1, and P2 in the model. (B) The middle ear structures isolated (Leckness et al., 2018).

1.4.2 FE Model of the Chinchilla Middle Ear

As mentioned previously, chinchilla is a commonly used animal model for hearing research. In 2016 the Biomedical Engineering Laboratory at the University of Oklahoma developed a FE model of the chinchilla ear to fully understand experimental observations through theoretical analysis. The model was based on X-ray micro-computed tomography (μCT) images and included the fluid domain in the ear canal and middle ear cavity, and the structural components consisting of the TM and TM annulus, ossicular chain and associated joints and suspensory ligaments, and mass block and dashpots to simulate the cochlear load. The septa, which are thin bony plates dividing the middle ear cavity and are unique to chinchilla, were also included. The FE model of the chinchilla ear is shown in **Figure 5**.

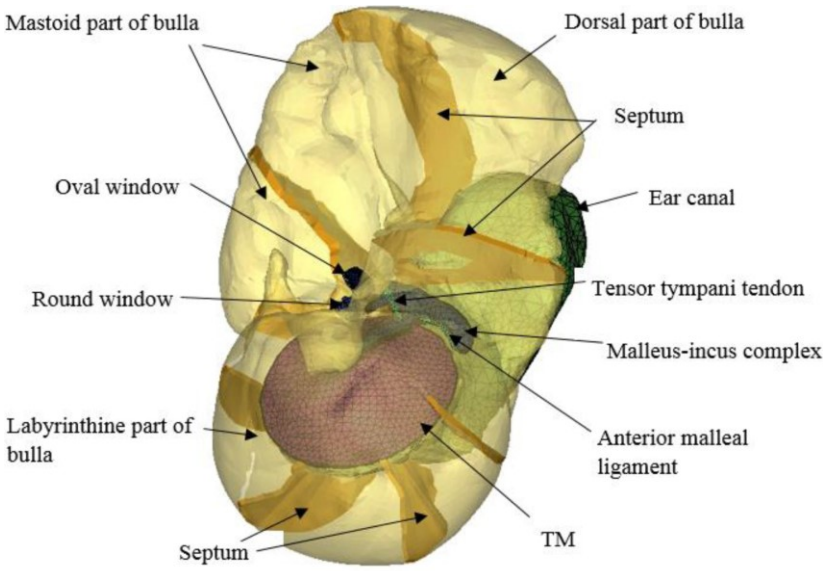

Figure 5. 3D FE model of the chinchilla ear developed by Wang & Gan (2016). This model was used to characterize middle ear functions in the frequency domain. Note that the cochlea was simulated by a mass block and dashpot system.

The model calculated the middle ear transfer function and middle ear admittance when a uniform sound pressure was applied in the ear canal. Acoustic-structure coupled behavior, similar to that used in the FE model of the human ear, was included in this model. The model-predicted TM displacement, stapes FP displacement, and middle ear admittance were validated with experimental data reported in the literature. This model was the first FE model of the chinchilla ear and was a step towards developing a comprehensive model. However, this model is limited by the lack of an anatomically correct cochlea, which would provide important information concerning the basilar membrane. Moreover, this analysis was handled in ANSYS APDL and studied middle ear functions in low-pressure conditions in the frequency domain.

In this thesis, the integration of a FE model of the chinchilla spiral cochlea with the model established by Wang & Gan (2016) was achieved. Harmonic analysis in ANSYS

Workbench was conducted to calculate middle ear functions. In addition, the geometry of this integrated model was extracted and modified to create a new model for the analysis of blast wave transmission in the transient domain.

1.5 Objectives

Service-connected auditory disabilities are prevalent among active Service members and Veterans and have a tremendous impact on quality of life. For these reasons, our understanding of the cause of hearing damage must be improved. Towards this goal, further studies investigating the effect of key blast parameters such as blast intensity, number of blast exposure, and recovery time are needed. To achieve this, a chinchilla animal model was established to investigate the effect of repeated low-intensity blast on progressive hearing loss in open and protected ears. Knowledge gained from this study may provide guidance for clinical evaluation and future research in blast-induced auditory dysfunction.

In addition, the creation of a FE model of the entire chinchilla ear, including spiral cochlea, would facilitate understanding of the anatomy and function relationship. Such a model is lacking in the literature and would be useful in future theoretical analyses. Moreover, this model may have future applications in translating experimental data from chinchilla exposed to blast to predict human response to blast.

Chapter 2: Auditory Dysfunction Induced by Repeated Low Intensity Blast Exposures in a Chinchilla Model

Repeated exposure to blast overpressure (BOP) waves is an inherent situation faced by Service members involved in many operational activities, especially the low-level military occupational blasts (MOBs) that do not result in loss of consciousness. Currently, the majority of studies on blast-induced hearing damage focus on relatively high intensity blasts. However, few studies have investigated the effects of repeated, low-intensity blast exposures on auditory function changes. This chapter reports our recent study to investigate the progressive hearing damage measured in chinchillas after repeated exposures to low-intensity blast.

2.1 Animal Model – Chinchilla

The chinchilla is a well-established animal model for investigating the effects of hearing loss and auditory function. The use of chinchilla as an animal model for hearing science is justified by numerous anatomical, behavioral, and physiological advantages. First and foremost, the chinchilla hearing sensitivity and frequency range overlaps significantly with humans, with an average hearing range of approximately 50 Hz to 33 kHz (Trevino et al., 2019). Other rodent models, such as mice and rat, can hear in the ultrasound. Furthermore, the chinchilla ear anatomy is similar to that of humans. Though the chinchilla does have an enlarged auditory bulla, this feature provides ease of access to the middle ear and cochlea, allowing for experimental manipulations to quantify sound transmission through the middle ear and into the cochlea (Trevino et al., 2019). Finally, the relatively docile and durable nature of the chinchilla permits the collection of a wide range

of physiological measurements. For these reasons, the chinchilla has seen widespread use in hearing research.

Healthy, young chinchillas (*Chinchilla laniger*) weighing between 500 and 800 g were included in this study. The study's protocol was approved by the Institutional Animal Care and Use Committee (IACUC) of the University of Oklahoma and met the guidelines of the National Institutes of Health (NIH) and the US Department of Agriculture (USDA). All animals were checked to be clear of disease in the ear upon arrival.

2.2 Experimental Design

Fourteen chinchillas were randomly divided into two groups (N = 7 each). Group 1 had standard foam earplugs (3M, Inc. St. Paul, MN) inserted deeply into the ear canal prior to blast, while no such hearing protection devices (HPDs, e.g. earplugs) were used in Group 2 animals. Both groups underwent a progressive study over 14 days with 6 blasts (5-10 min intervals between blasts) on Day 1. **Figure 6** is an overview of the experimental procedures for the two groups.

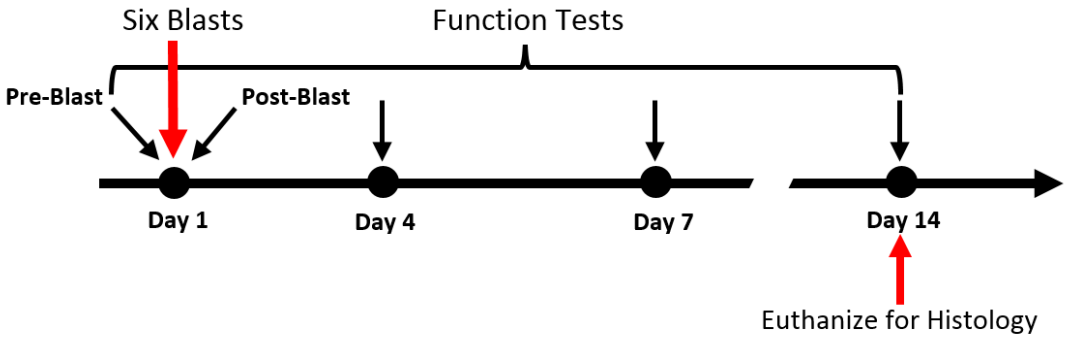

Figure 6. Timeline of experimental procedures. Key experimental procedures (e.g. blasts, function tests, and euthanasia) are labeled at the time points they occurred.

The animals were anesthetized with 35 mg/kg Ketamine and 7 mg/kg Xylazine to ensure the chinchilla was sedated throughout the duration of the experiment. Each ear was examined using a surgical endoscope (Straight Endoscope, Stryker, MI) to verify that no TM or middle ear abnormalities existed. The auditory brainstem response (ABR), distortion product optoacoustic emissions (DPOAE), and middle latency response (MLR) function tests were conducted prior to blast exposure to measure the baseline of the hearing function of each animal.

After pre-blast function tests were conducted, the animal was placed in a specifically designed L-shape animal holder and fixed using straps. The animal's body was positioned so that the top of the animal's head faced the blast source (**Figure 7**). A pressure sensor (Model 102B16, PicoCoulomB Piezotronics, Depew, NY) was fixed on the animal holder near the canal entrance to monitor the blast pressure at the entrance of the ear canal. A standard foam earplug (3M, Inc. St. Paul, MN) was then inserted into both ears of Group 1 animals. It should be noted that the sensor at the entrance of the ear canal was not in contact with the earplug in the canal.

A well-controlled compressed nitrogen-driven blast apparatus located inside an anechoic chamber in the Biomedical Engineering Laboratory at the University of Oklahoma (**Figure 7**) was used to create BOPs in this study (Engles et al., 2017). Polycarbonate films (McMaster-Carr, Atlanta, GA) of 0.25 mm were utilized to generate the BOP level. In this study, animals were exposed to a BOP level of 3-5 psi (21-35 kPa). Animals were exposed to 6 repeated blasts, with approximately 5 minutes between blasts.

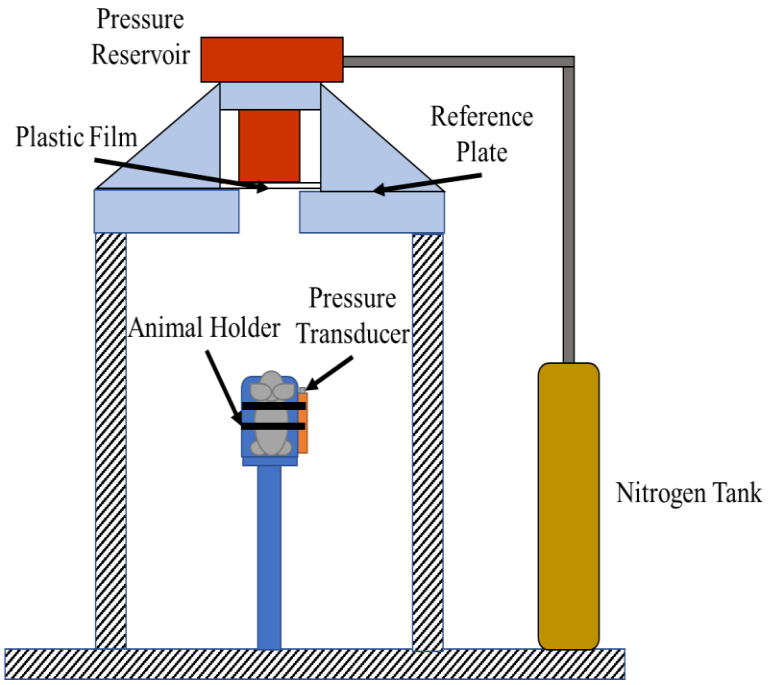

Figure 7. Schematic of animal experimental setup with blast apparatus. The animal was held in place in a specifically designed holder and exposed to 6 repeated low-level BOPs. BOP level was monitored by the pressure transducer near the animal ear (Smith et al., 2020).

The pressure sensor signals were collected by a cDAQ 7194 and A/D converter 9215 (National Instruments Inc., Austin, TX) with a sampling rate of 100k/s (10 ms dwell time). The LabVIEW software package (NI Inc) was used for data acquisition and analysis. The waveform of each blast was saved to a PC for further analysis. Note that the sampling rate is sufficient for the waveform recorded in this study. After the completion of blast exposure, the status of the chinchilla TM was examined using an endoscope before post-blast auditory function tests were conducted. Animals were then observed for fourteen days.

2.3 Hearing Function Tests

Auditory function measurements including auditory brainstem response (ABR), distortion product otoacoustic emissions (DPOAE), and middle latency responses (MLRs) were recorded pre- and post-blast on Day 1 and then again on Days 4, 7, and 14. During the function tests, animals remained under anesthetic as described above.

2.3.1 Auditory Brainstem Response (ABR)

Differences in ABR threshold reflected hearing level changes after blast exposure in chinchillas. An increase in ABR threshold is indicative of hearing damage. The ABR measurements were recorded in both ears using a TDT system III (Tucker-Davis Technologies, Alachua, FL) following protocol previously established in our studies (Gan et al., 2016). Briefly, chinchillas were placed under anesthesia and stainless steel needle electrodes were inserted subcutaneously at the vertex of the skull and ventrolateral surfaces of the ear, while a ground electrode was positioned in the rear leg. Tone burst stimuli of 1 ms rise/fall time at frequencies of 0.5, 1, 2, 4, 6, and 8 kHz were generated, which is in accord with a widely-accepted frequency range for chinchilla studies (Gan et al., 2016; Zhong et al., 2014) . The ABR waveforms were recorded in descending 5 dB SPL intervals from the maximum amplitude of 100 dB SPL until no waveform could be identified. If an ABR response was not detected at the maximum acoustic stimulation, the threshold was set to 100 dB.

2.3.2 Distortion Product Otoacoustic Emissions (DPOAE)

DPOAE was measured using the TDT system III to evaluate the cochlear outer hair cell function as described in Chen et al. (Chen et al., 2019). In this study, the DPOAE level shifts after blast exposure were measured in Group 1 animals (i.e., chinchilla with HPDs). Cubic 2f1-f2 DPOAE levels were recorded using two primary tones, f1 and f2, presented at primary tone levels of L1 = 70 dB SPL and L2 = 65 dB SPL (Daniel et al., 2007). A probe tipped microphone (ER-10B, Etymotic Research) was sealed in the animal's external ear canal to capture DPOAE recording at 2f1-f2 (f2 = 1.22xf1). The DPOAE levels were defined as the signal/noise ratio of the 2f1-f2 distortion product for the 70 dB and 65 dB SPL of f1 and f2 primaries, respectively, and were calculated by subtracting the 2f1-f2 distortion product form the surrounding noise. DPOAE level shifts were calculated by subtracting post-exposure from pre-exposure values.

2.3.3. Middle Latency Responses (MLR)

Middle latency responses provide insight into the neurological function of the higher CAS, reflecting part of the central auditory cortex function (Torre & Fowler, 2000). Four characteristic components of MLR waveforms include two negative voltage waves (Na and Nb) and two positive voltage waves (Pa and Pb). The latencies and amplitudes of the Pa (positive) and Na (negative) peaks reflect the neural conduction velocity from the peripheral auditory nerve to the central auditory nervous system. The Pa component of the MLR originates from the inferior colliculus within the midbrain region, while the Na component arises from the subcortical and cortical regions of the auditory system. Thus,

MLR tests were used as an indicator of damage to the central auditory nerve pathway after blast exposure.

MLRs were recorded using short click and tone stimuli presented at a rate of 4/sec and with a 100 ms long recording window (TDT system III). Thus, early components (< 10 ms) of the wave form collected under the MLR acquisition settings were responses from ABR generator regions, while later responses correspond to the more central generators in the thalamus and cortex (Arnold, 2000). Chinchillas show an acoustic MLR wave with one negative peak (Na) with a high amplitude wave at 14-18 ms and one positive peak (Pa) with a high amplitude wave at 19-35 ms in response to the click sound. MLRs recorded from the interaural line (channel 2) were analyzed. Brief 0.5 kHz tones (2 ms in duration) of alternating polarity were used in MLR recording (Race et al., 2017).

2.4 Statistical Analysis

The ABR, DPOAE, and MLR measurement data were expressed as the mean ± SEM and plotted in GraphPad Prism (GraphPad Software Inc., Version 8). The unpaired t-test was used to compare the ABR threshold shifts, MLR latencies (Na and Pa), and MLR amplitudes of the protected ear and unprotected ear groups. The paired t-test was used to compare the DPOAE level shifts measured on D1 and D14. Values of $P < 0.05$ were considered statistically significant.

2.5 Results

2.5.1 BOP Waveforms

Figure 8 shows a typical waveform of BOPs in units of psi (1 psi = 6.9 kPa) measured at the entrance of the ear canal over a time of 10 ms. The waveform shown

illustrates a single positive overpressure peak at a level of 4.0 psi. After reaching the sharp positive peak, the pressure quickly decreased to a level of -1.6 psi and then returned to 0 psi. The BOP waveforms were repeatable for each blast test.

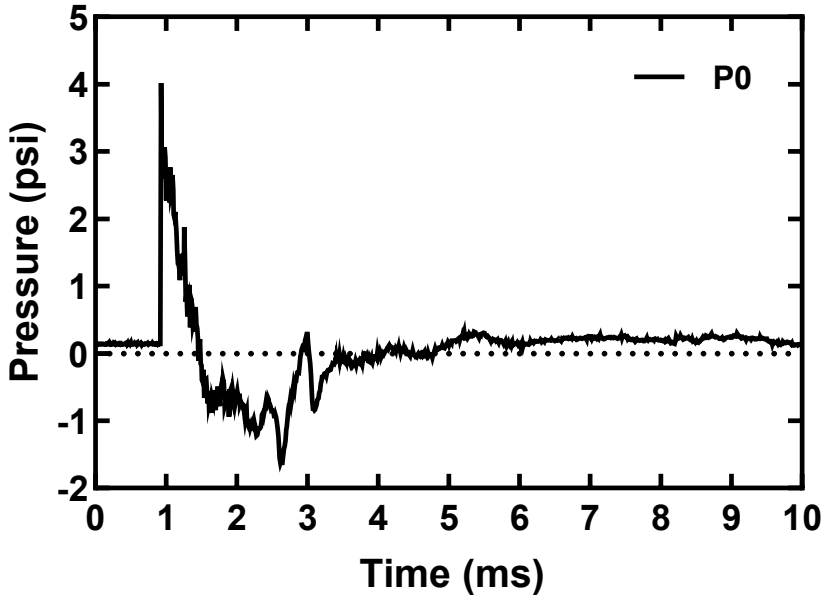

Figure 8. A recorded BOP waveform at the entrance of the ear canal from an animal test with earplugs with a peak pressure of 4.0 psi.

2.5.2 ABR Threshold Shifts

The mean and SEM of the ABR threshold shifts measured from animals in Group 1 (N = 7) and in Group 2 (N = 7) over a 14-day period after blast exposures are shown in **Figure 9**. The ABR threshold shifts measured from plugged ears immediately after blasts on Day 1 (D1), and those measured after 4 days (D4) and 14 days (D14) post-blasts are shown in **Figure 9A**. The greatest threshold shift occurred on Day 1, ranging from approximately 30 dB at 1 kHz to around 50 dB at 8 kHz, and decreased over time. By Day 14, the ABR threshold shift level was roughly 10 dB across all frequencies.

Figure 9B shows the ABR threshold shifts recorded from unprotected or open ears at the same time points as those seen in **Figure 4A**. Similar to the ABR threshold shifts of the plugged ears, the ABR threshold shifts of the open ears were also the greatest on Day 1, ranging from about 37 dB at 1 kHz to approximately 50 dB at 8 kHz, and also decreased over time. However, the ABR threshold shifts of the open ears were greater than those of the plugged ears on Days 4 and 14, indicating greater damage in open ears than in protected ears. Moreover, while the threshold shift of plugged ears had decreased to about 10 dB across all frequencies by Day 14, the threshold shift of open ears ranged from 15 dB at 1 kHz to 30 dB at 8 kHz.

The data from plugged and open ears on Days 1, 4, and 14 are compared in **Figure 9C**. As shown in **Figure 9C**, the hearing threshold shift in plugged ears (dashed lines) slowly decreased over the 14-day time period. However, some hearing loss was still observed at Day 14 (bottom dashed line). Open ears (solid lines) exhibited some recovery by Days 4 and 14, but the ABR threshold shift remained elevated at 20-35 dB on Day 4 and 15-30 dB on Day 14. The ABR threshold shifts were significantly different between the two groups at 4 kHz on Day 4 and at 4, 6, and 8 kHz on Day 14. Overall, this data suggests that permanent hearing damage occurred in both unprotected and protected ears, but to a greater extent in unprotected ears.

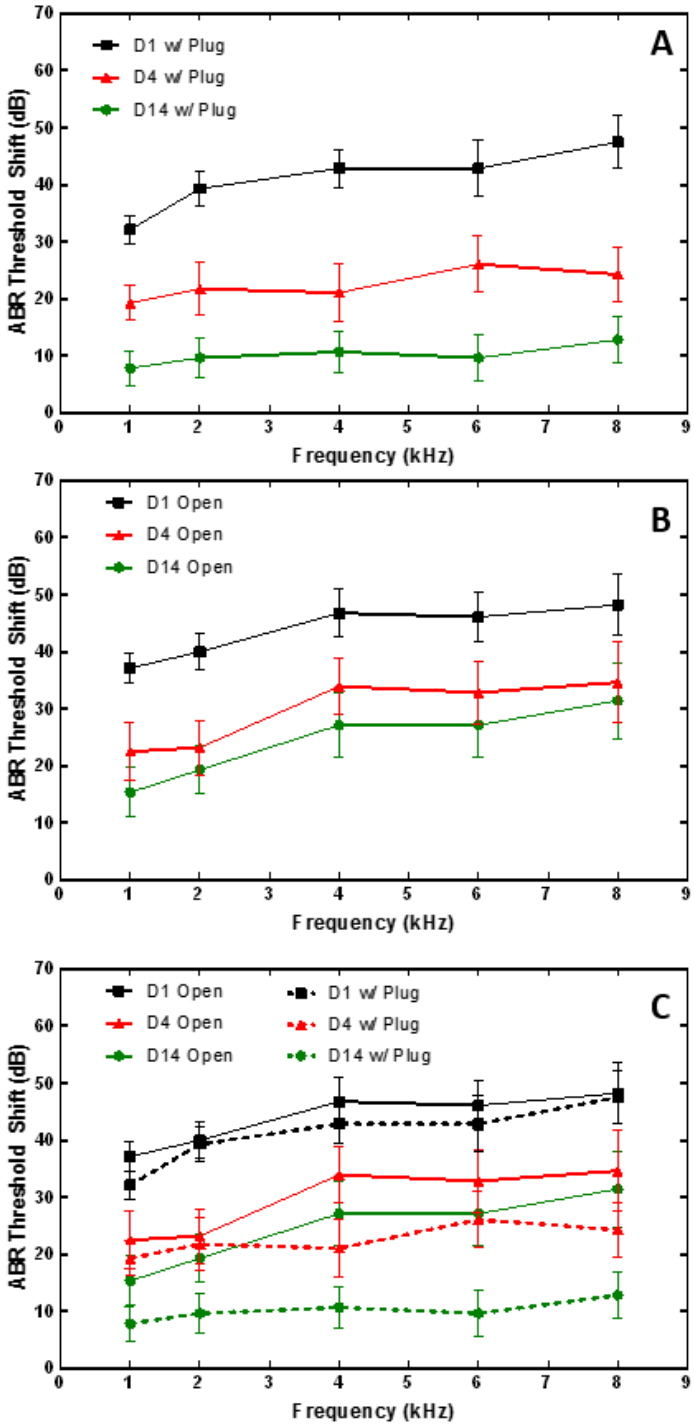

Figure 9. (A) ABR threshold shifts (mean ± SEM, n = 14 ears) measured in plugged ears after 6 blasts on Day 1, Day 4, and Day 14. (B) ABR threshold shifts (mean ± SEM, n = 14 ears) measured in open ears after 6 blasts on Day 1, Day 4, and Day 14. (C) Comparison of ABR threshold shifts in plugged and open ears on Days 1, 4, and 14.

2.5.3 ABR Wave I Amplitudes

The ABR wave I amplitudes (peak-to-peak amplitudes) measured from animals with and without earplugs on Day 1 (pre- and post-blast), Day 4, and Day 14 after blast exposures are shown in **Figure 10**. The mean and SEM values were plotted against the level of acoustic stimulus from 40 to 100 dB SPL measured in chinchilla ear canal. ABR wave I amplitudes measured at frequencies of 1, 2, 4, and 8 kHz from plugged and open ears were presented in different subplots. The top row of **Figure 10** for unprotected ears indicates a considerable reduction in wave I amplitude post-blast across all frequencies. The curves for Day 4 and Day 14 demonstrate some recovery from damage from 1-4 kHz but remained slightly lower than the pre-blast curve. The difference between pre-blast and Day 4 and 14 curves is more pronounced at 8 kHz, suggesting some permanent damage of the wave I amplitude at high frequencies in open ears.

The bottom row of **Figure 10** for plugged ears also displays a decrease in post-blast wave I amplitude across all frequencies, though not as substantial as the difference shown in open ears for the same time points. Furthermore, the results obtained on Days 4 and 14 show little difference from the pre-blast data from 1-4 kHz, and only a slight difference at 8 kHz. These results indicate that repeated blasts at this BOP level induced a temporary reduction in the wave I amplitude in protected ears. In contrast to open ears, Day 14 results for protected ears show recovery to pre-blast conditions, demonstrating that earplugs may have prevented permanent damage to cochlear ribbon synapses, spiral ganglion neurons, and auditory neural fibers.

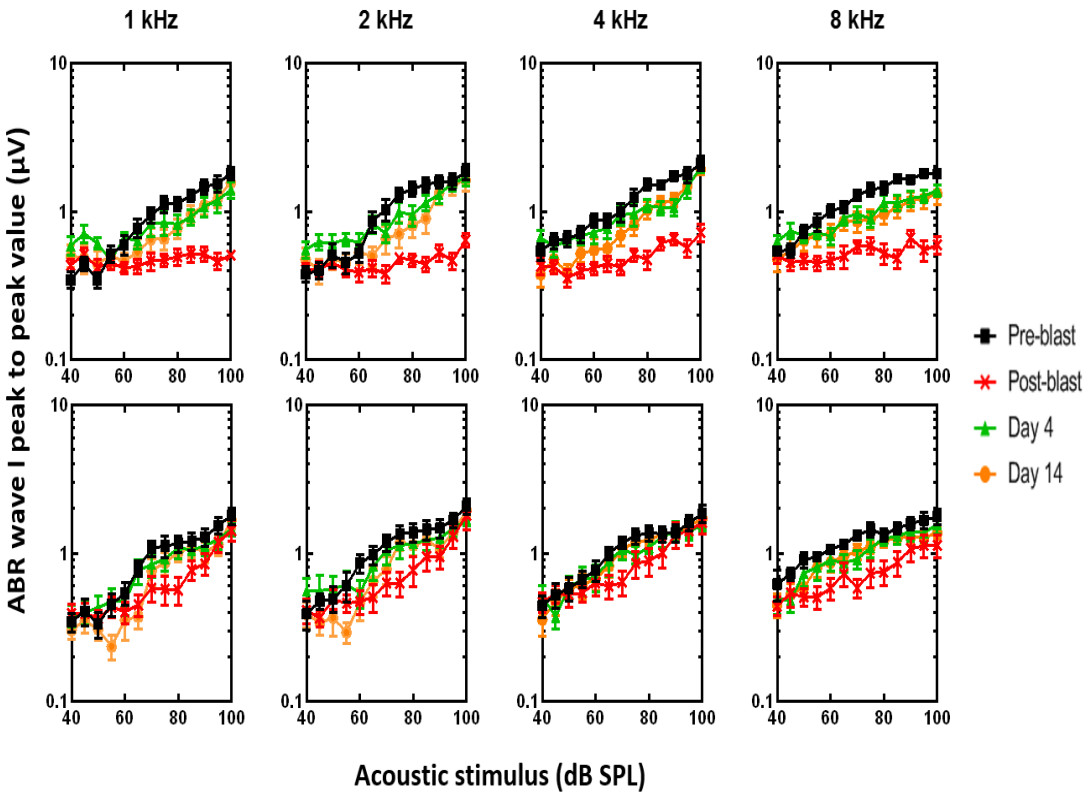

Figure 10. ABR wave I amplitude in response to stimulus level from 40 to 100 dB SPL measured from (top) open ears (mean ± SEM, n = 14 ears) and (bottom) plugged ears (mean ± SEM, n = 14 ears). Measurements were taken at frequencies of 1, 2, 4, and 8 kHz.

2.5.4 DPOAE Level Shifts

The mean and SEM of DPOAE level shifts (reductions) measured from animals in Group 1 on Day 1 (D1) and Day 14 (D14) at frequencies of 1-14 kHz is shown in **Figure 11**. The mean values of the DPOAE level shifts increased from about 7 dB SPL at 1 kHz to a peak of 33 dB at 11 kHz on Day 1. The shift decreased substantially on Day 14 to around zero dB at 1 kHz and below 10 dB over the rest of the frequency range. The DPOAE results on Day 1 and Day 14 were significantly different across all frequencies. The results obtained from plugged ears indicate that the protection of earplugs may have facilitated the

recovery and prevented the permanent loss of the outer hair cells in the cochlea to some degree.

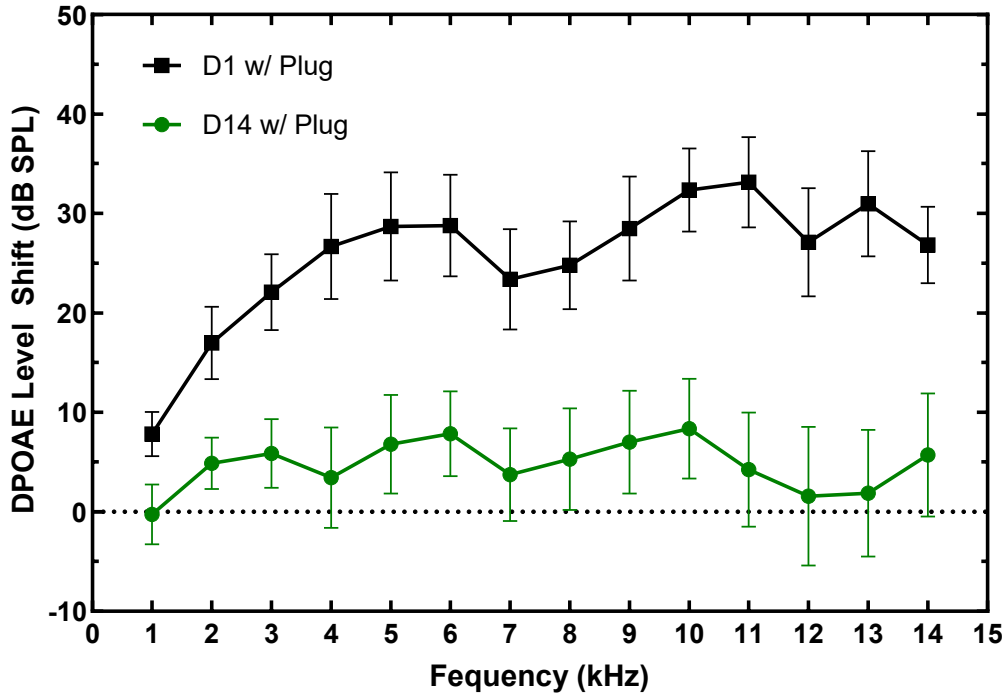

Figure 11. DPOAE level shifts (mean ± SEM, n = 14 ears) measured from protected ears on Days 1 and 14.

2.5.5 Assessment of Central Auditory System Damage (MLRs)

Representative curves of MLR signals in unprotected ears over the 14-day time period are shown in **Figure 12**. MLR traces were recorded at 80 dB SPL with the stimulate frequency of 0.5 kHz. The pre-blast waveform is comprised of a negative peak (Na peak) at 14-18 ms and a positive peak (Pa peak) at 19-22 ms. The amplitudes and time latencies of the Pa and Na peaks reflect the condition of the central auditory nervous system.

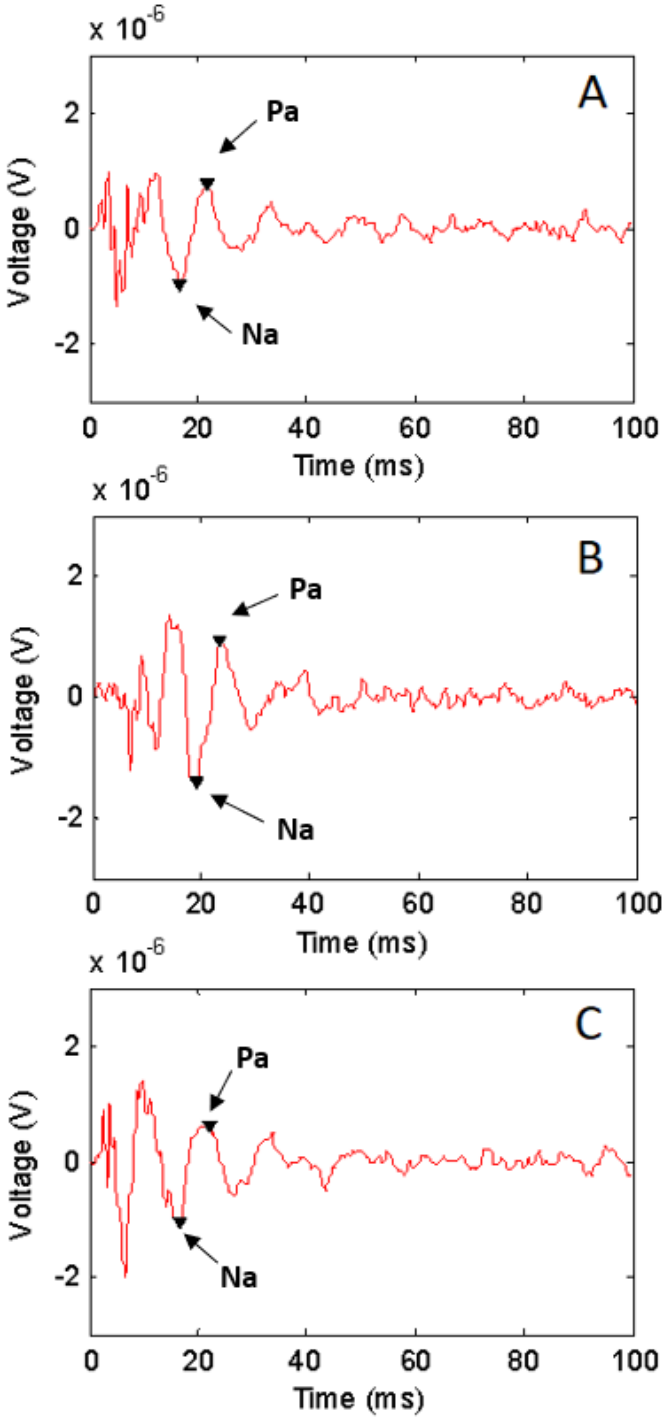

Figure 12. Representative MLR traces from chinchilla with unprotected ears taken (A) pre-blast (B) post-blast and (C) Day 14. Traces were recorded at 80 dB SPL with a stimulate frequency of 0.5 kHz. The Na peak and Pa peak are indicated by arrows.

The mean ± SEM peak-to-peak amplitude measured from Na to Pa, Na latency, and Pa latency for the protected and unprotected ears are summarized in **Figure 13**. **Figure 13A** shows the peak-to-peak amplitude for protected and unprotected ears pre-blast to be 2.71 ± 0.28 μV and 2.29 ± 0.16 μV, respectively. After the blast exposures, the average peak-to-peak amplitude in protected ears and unprotected ears decreased to 2.09 ± 0.49 μV and 1.85 ± 0.39 μV, respectively. On Day 14 (D14), the peak-to-peak amplitudes for protected and unprotected ears had further reduced to 1.43 ± 0.12 μV and 1.53 ± 0.27 μV, respectively. There were no significant differences between the peak-to-peak amplitudes of the protected and unprotected ears. This data indicates that there was damage to the CAS in both protected and unprotected ear groups that was not resolved over 14 days.

Figure 13B shows the average Na peak latency in protected and open ears. Before blast exposure, the average Na peak latencies in protected and open ears were determined to be 15.70 ± 0.83 ms and 16.33 ± 0.22 ms, respectively. The Na latencies for both plugged and open ears increased after blast to 18.50 ± 0.30 ms and 18.17 ± 0.76 ms, respectively. By D14, the Na latencies for protected and open ears had reduced to 17.1 ± 0.13 ms and 17.1 ± 0.46 ms, respectively. However, these values were slightly elevated in comparison to their respective pre-blast values, suggesting that there may still be damage to the CAS. It should be noted that there were no significant differences between the Na latencies of the protected and unprotected ears.

The average Pa peak latency in open and protected ears over a 14-day time period is displayed in **Figure 13C**. Prior to exposure to repeated blasts, the Pa latencies for protected and open ears were determined to be 21.71 ± 0.81 ms and 21.14 ± 0.26 ms, respectively. After blast, the latency of the Pa peak increased to 22.80 ± 0.44 ms and 22.76

± 0.87 ms for protected and unprotected ears, respectively. The Pa peak latencies for both plugged and open ears returned to roughly pre-blast levels by D14, however, at 21.38 ± 0.61 ms and 21.43 ± 0.55 ms, respectively. There were no significant differences between the Pa latencies of the plugged and open ears.

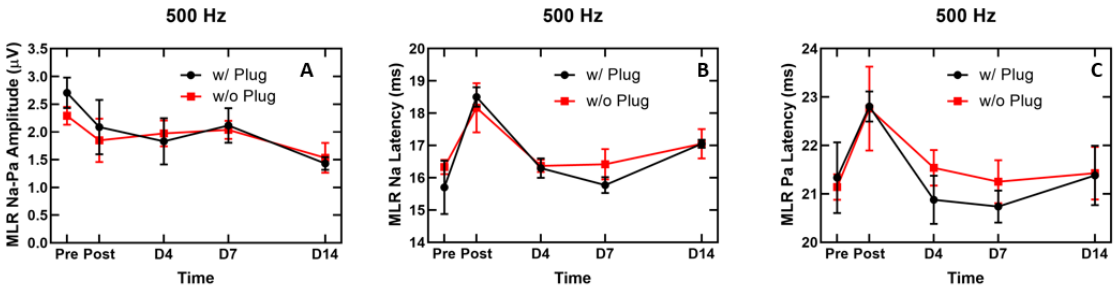

Figure 13. MLR results at 500 Hz at 80 dB SPL in open (mean ± SEM, n = 6 ears) and protected ears (mean ± SEM, n = 4 ears) after exposure to 6 consecutive low-intensity blasts of 21-35 kPa (3-5 psi). (A) Peak-to-peak amplitude measured from Na to Pa. (B) Na latency and (C) Pa latency.

2.5.6 Discussion

2.5.6.1 Hearing Damage Induced by Repeated Low-Intensity BOPs

In this study, the ABR thresholds for animals in both Group 1 and Group 2 were substantially elevated after repeated blast exposures. While the ABR threshold shifts did decrease with time over 14 days in both protected and unprotected ears, they did not recover to their respective pre-blast levels (**Figure 9**). These findings suggest that the hearing recovery was limited in both protected and unprotected ears.

The MLR measurements are a reflection of the recovery process of the CAS after repeated blast exposure. As shown in **Figure 13A**, after blast the peak-to-peak MLR amplitudes were reduced for both groups, indicating that some damage to the CAS had occurred. By D14, the amplitude levels of both groups were still less than the pre-blast

levels, suggesting that the CAS had not fully recovered. The Na latency values for both groups increased after blast. However, the latency times for both groups demonstrated a gradual decrease over 14 days. The Pa latency values for both groups exhibited a similar trend, rising sharply after blast but then returning to roughly the original pre-blast values. There were no significant differences between the MLR measurements for the plugged and open ear groups. Collectively, these results suggest that exposure to 6 repeated low-intensity blasts induced some degree of dysfunction in the CAS and indicate that the protective mechanism of earplugs may be limited for the CAS when exposed to repeated low-intensity blasts.

ABR wave I signal, which is a predictive indicator of cochlear synaptopathy (Hickman et al., 2018; Liberman & Kujawa, 2017), was also measured in this study. In open ears, decreased wave I amplitudes were observed after repeated blast exposure. Wave I amplitudes for open ears were lower than the pre-blast amplitudes even after 14 days, indicating that there may have been strong acute cochlear synaptopathy that was not resolved completely in the long-term. Wave I amplitudes for protected ears also suggested acute cochlear synaptopathy, though not to the degree of that observed in open hears. However, wave I amplitudes for protected ears appeared to recover over 14 days.

2.5.6.2 Effect of Number of Blasts and HPDs

Recently, a similar study in which chinchillas with and without HPDs were exposed to 3 BOPs of 3-5 psi and evaluated for progressive hearing damage over 7 days (Chen et al., 2019). The results reported in this study and in Chen et al. (2019) are compared to investigate the effect of the number of blasts and HPDs. As seen in **Figure 14**, chinchillas

without HPDs that were exposed to 6 repeated blasts experienced a greater ABR threshold shift than their counterparts exposed to 3 repeated blasts. This trend is also reflected in the ABR threshold shifts of chinchillas with earplugs after exposure to 3 or 6 repeated blasts (**Figure 15**). Thus, ABR threshold shifts indicate that chinchillas exposed to 6 repeated blasts, regardless of hearing protection condition, experienced greater hearing damage than those exposed to fewer blasts.

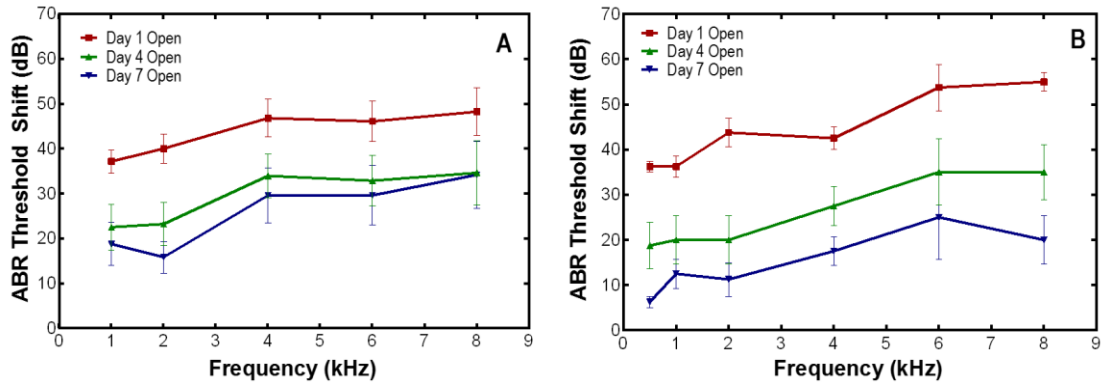

Figure 14. ABR threshold shifts (mean ± SEM) measured in open ears on Days 1, 4, and 7 after exposure to low-intensity blasts of 21-35 kPa (3-5 psi). (A) 6 consecutive blasts (n=14) and (B) 3 consecutive blasts (n=7) (Fig. 5B, Chen et al. 2019).

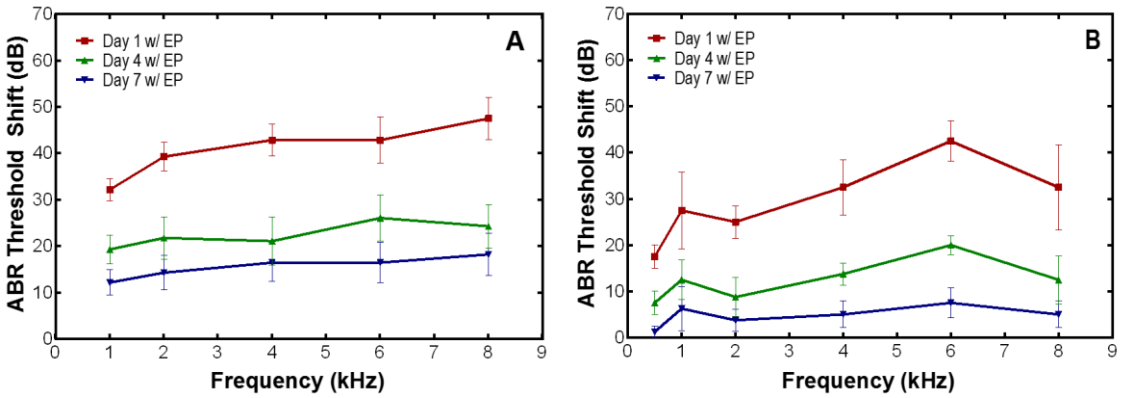

Figure 15. ABR threshold shifts (mean ± SEM) measured in protected ears on Days 1, 4, and 7 after exposure to low-intensity blasts of 21-35 kPa (3-5 psi). (A) 6 consecutive blasts (n=14) and (B) 3 consecutive blasts (n=7) (Fig. 5A, Chen et al. 2019).

Comparison of the results from Chen et al. (2019) and those presented herein provide insight into the ability of earplugs to reduce hearing damage. In comparing **Figure 14A** and **Figure 15A**, results demonstrate that the hearing threshold of animals with protected ears recovered to a greater extend by D7 than those without earplugs after exposure to 6 repeated blasts. Chinchillas with and without HPDs exposed to 3 repeated blasts also demonstrated a similar trend (**Figure 14B** vis **Figure 15B**).

ABR wave I results from both studies suggest that both 3 and 6 repeated blasts were enough to induce cochlear synaptopathy in chinchillas without earplugs (**Figure 16A-B**). By D7, the ABR wave I amplitudes for open ears exposed to 3 and 6 blasts were still reduced at 8 kHz. In contrast, the ABR wave I peak-to-peak value for chinchillas with earplugs (**Figure 16C-D**) from both studies had recovered to a greater degree than their respective unprotected counterparts. However, those exposed to 6 repeated blasts demonstrated a greater acute ABR wave I decrease than those exposed to 3 repeated blasts, which aligns with the results from the ABR threshold shifts.

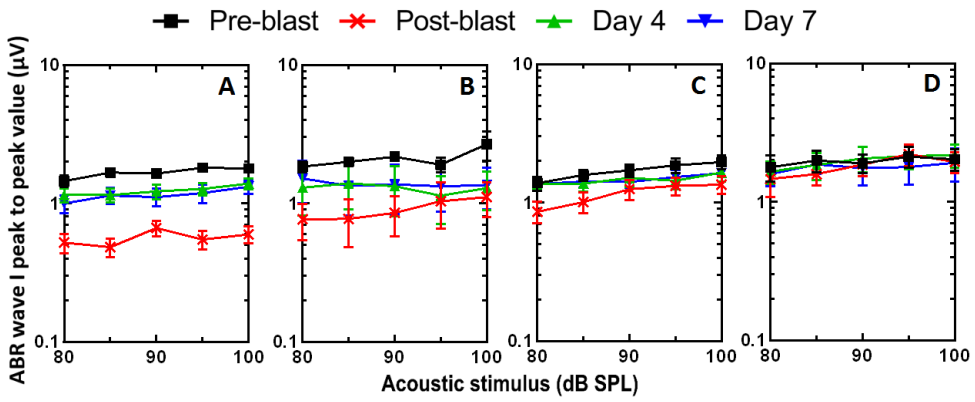

Figure 16. ABR wave I amplitude (mean ± SEM) in response to stimulus level from 80 to 100 dB SPL measured from (A-B) open ears and (C-D) protected ears after exposure to low-intensity blasts of 21-35 kPa (3-5 psi). (A, C) 6 consecutive blasts (n=14) and (B, D) 3 consecutive blasts (n=7) (Fig. 6, Chen et al. 2019). Measurements were taken at 8 kHz.

Finally, differences in DPOAE results measured from animals with earplugs may be attributed to differences in the number of blast exposures. Results from Chen et al. (2019) and the study reported herein indicate that chinchilla exposed to 6 repeated blasts had slightly greater disruption of outer hair cell function than those exposed to 3 repeated blasts, as evidenced by the greater increase in DPOAE level shifts shown in **Figure 17**. 6-blast animals demonstrated greater acute damage on D1, particularly in the 3-6 kHz region than 3-blast animals. By D7, the DPOAE level of 3-blast animals had recovered to a greater degree than 6-blast animals, especially at mid-frequencies.

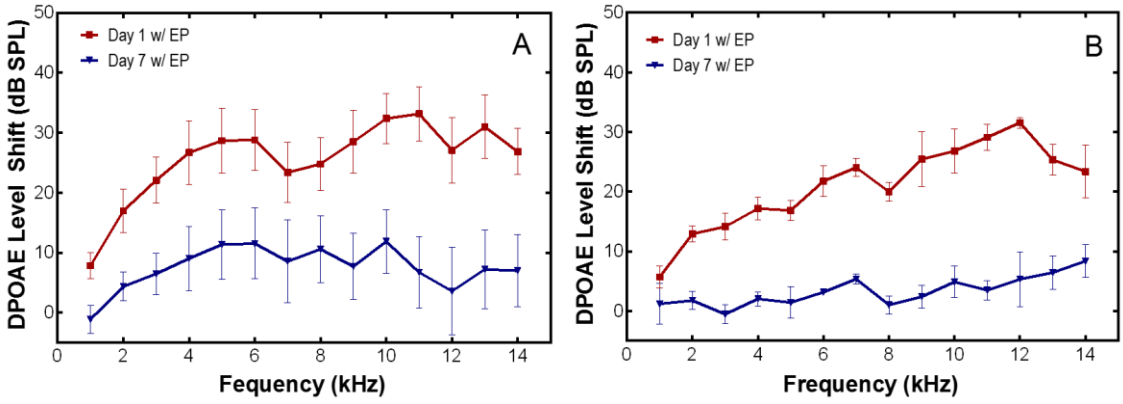

Figure 17. DPOAE level shifts (mean ± SEM) measured from protected ears on Days 1, 4, and 7 after exposure to (A) 6 consecutive blasts (n=14) and (B) 3 consecutive blasts (n=7) (Fig. 7A, Chen et al. 2019).

2.6 Chapter Summary

This study aimed at investigating the progressive hearing damage in chinchillas when exposed to repeated low-intensity blasts. Animals with and without earplugs were exposed to low-level blast overpressure of 3-5 psi (21-35 kPa). ABRs, DPOAEs, and MLRs were measured pre- and post-blast and over a time period of 14 days for the progressive study. Major findings from this study include: 1) overall, 6 blasts were able to

induce permanent hearing damage in both open and protected ears, suggesting that HPD function was limited under conditions of repeated low-intensity blast; 2) hearing function tests indicate dysfunction in both the peripheral and central auditory systems; 3) 6 low-intensity blasts induced greater hearing damage in protected and unprotected ears than in protected and unprotected ears exposed to 3 low-intensity blasts of equal BOP level.

Chapter 3: 3D FE Model of Chinchilla Ear for Acoustic Sound Transmission

The FE model of the chinchilla ear previously reported in literature focused on the middle ear. While the outer and middle ear portions of this model were based on X-ray (μCT) images, the cochlea itself was simulated by a mass block and dashpots. Furthermore, the FE analyses of this model used ANSYS APDL (ANSYS Classic) to calculate the response of the middle ear to a uniform acoustic pressure in the frequency domain.

This chapter will discuss the creation of the chinchilla cochlea model and its integration with the existing middle ear model. Furthermore, the transition from ANSYS APDL to ANSYS Workbench to simulate acoustic sound transmission will be detailed. The applied boundary conditions and material properties will be described as well. The results obtained from the model will be presented and compared with published data for model validation.

3.1 Creation of 3D FE Model of Chinchilla Ear

This section will discuss the previously published 3D FE model of the chinchilla middle ear. Then, the creation of the FE model of the chinchilla cochlea will be described. Finally, integration of both models into one cohesive model will be detailed.

3.1.1 3D FE Model of the Chinchilla Middle Ear

Harmonic analysis over the auditory frequency range of 100-10,000 Hz was conducted in a 3D FE model of the chinchilla middle ear (Wang & Gan, 2016). Based on X-ray (μCT) images of an adult chinchilla bulla (**Figure 18**), the 3D FE model included

the TM, ossicular chain and associated suspensory ligaments (C1, C3, C5, and C7), bony septa, and middle ear cavity. The air in the ear canal and middle ear cavity were meshed by acoustic elements, while the middle ear structures were meshed by solid elements. All elements in this model were four-node elements. The FE model of the chinchilla middle ear is shown in **Figure 19.**

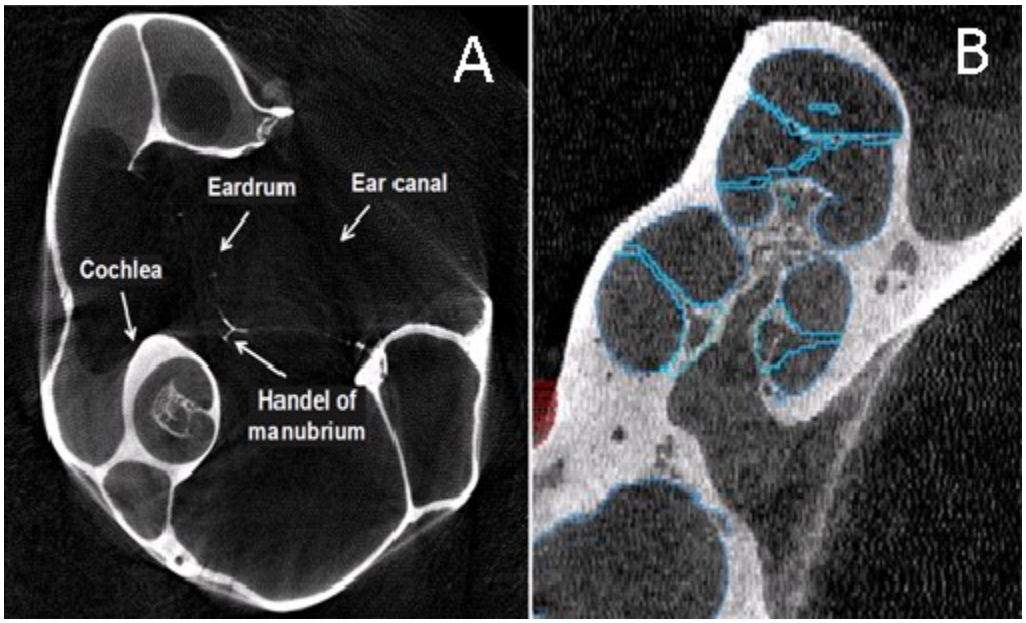

Figure 18. (A) A typical μCT image of a chinchilla left ear with (B) bony structure outlined in blue (Wang & Gan, 2016). Characteristic structures of the ear such as the cochlea are labeled.

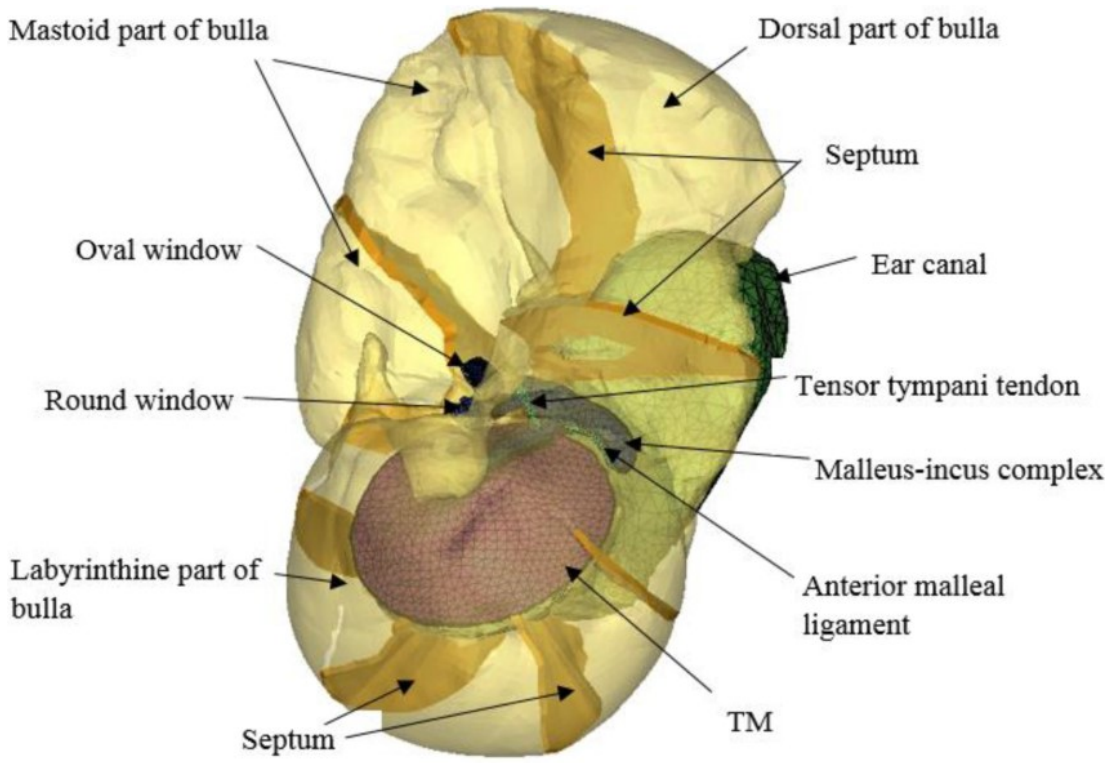

Figure 19. 3D FE model of the chinchilla middle ear (Wang & Gan, 2016). Key structures of the chinchilla ear are labeled. Note that this model did not include an anatomically accurate model of the cochlea.

3.1.2 Chinchilla Cochlea Model

The chinchilla cochlea model was constructed in a similar manner to the middle ear model. X-ray (μCT) slices were used to identify the cochlea and a geometry model was built in Amira. The surfaces of the geometry model built in Amira were then translated into HyperMesh (Altair Computing, Inc., Troy, MI) to generate FE meshes of the cochlea. As shown in **Figure 20** and **Figure 21**, the FE model of the chinchilla cochlea is comprised of two fluid filled chambers, the scala tympani and scala vestibule, which are separated by the basilar membrane and connect at the helicotrema. The two and a half turn cochlea consisted of a total of 28,170 elements, with the scala tympani and scala vestibuli

composed of 12,816 elements and 12,834 elements, respectively. **Figure 21** depicts the basilar membrane and its bony supports, which in total consisted of 1,602 elements. The basilar membrane was approximately 16 mm in length. **Figure 22** shows the basilar membrane within the cochlear fluid.

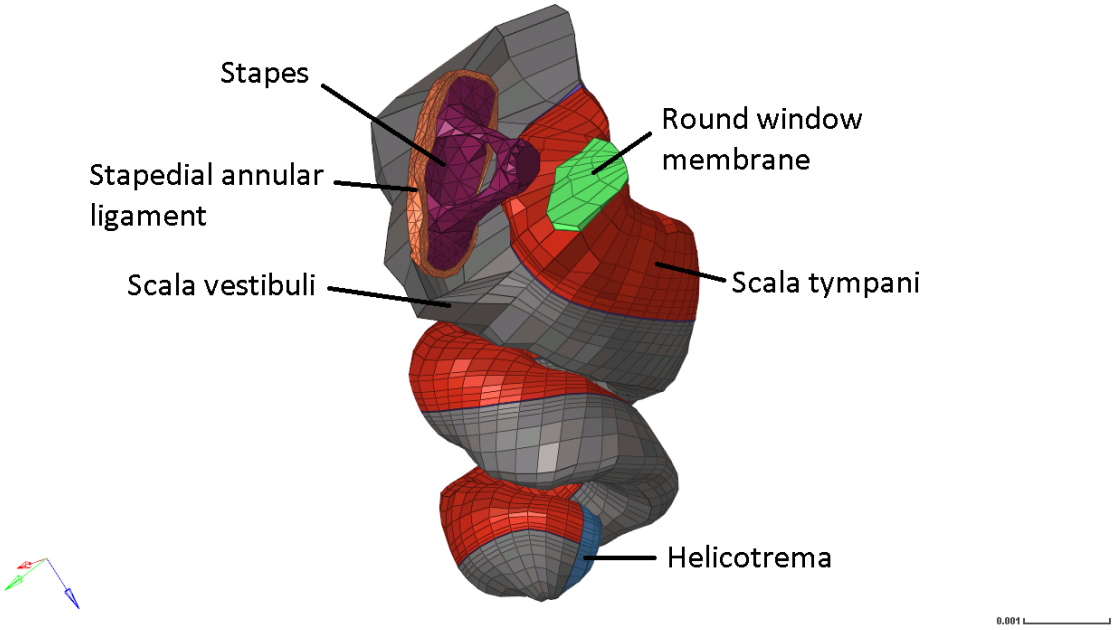

Figure 20. FE model the chinchilla cochlea with middle ear components (stapes, stapedial annular ligament, and round window membrane) to illustrate connection points to the middle ear model. The global coordinate system is shown (x – red, y – green, z – blue). The scale bar is 0.001 m.

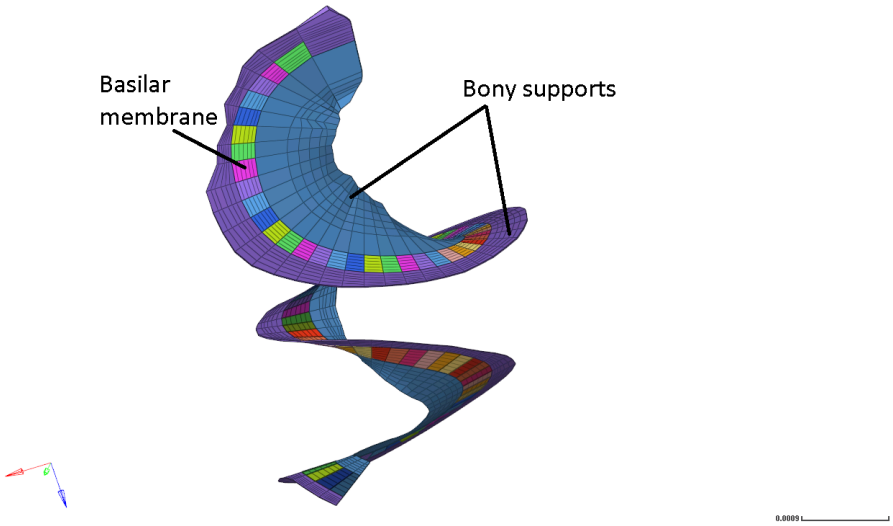

Figure 21. Basilar membrane structure and associated bony supports of the FE model of the chinchilla cochlea. The basilar membrane was approximately 16 mm in length. The scale bar is 0.0009 m.

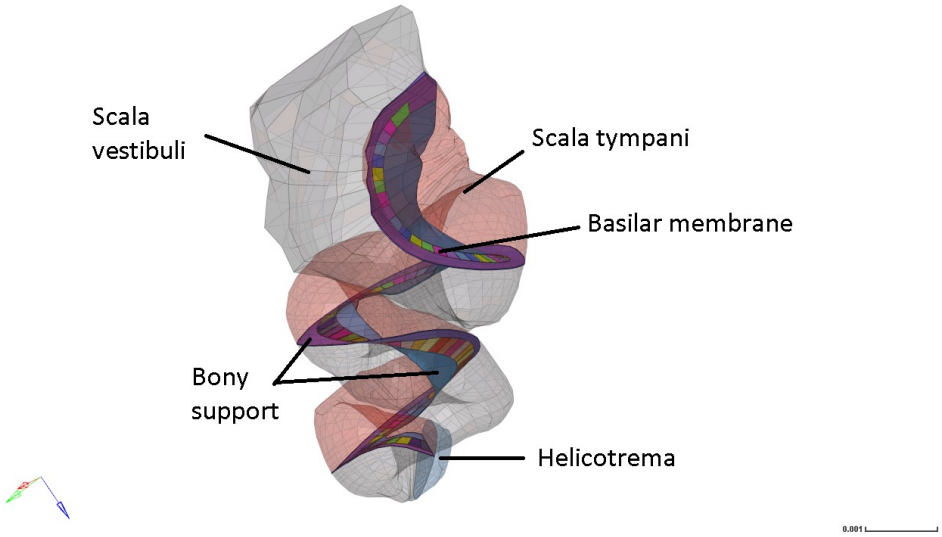

Figure 22. Basilar membrane and associated bony supports surrounded by cochlear fluid (transparent). Note that the basilar membrane separates the scala tympani and scala vestibuli. These two fluid filled chambers connect at the helicotrema. The scale bar is 0.001 m.

3.1.3 Creation of 3D FE Model of Chinchilla Ear

The FE models of the chinchilla middle ear and chinchilla cochlea were integrated into one cohesive model in HyperMesh. The stapes and round window membrane structures of the middle ear were connected to the cochlea and the nodes at the interfaces were equivalenced. The integrated 3D FE model of the entire chinchilla ear is shown below in **Figure 23**. Note that the septa (thin bony plates that divide the middle ear cavity into two chambers) are omitted for viewing purposes. **Figure 24** emphasizes the septa structures found in the middle ear cavity. The TM, ossicular structures and associate supporting ligaments, and cochlea components of the model are shown in **Figure 25**.

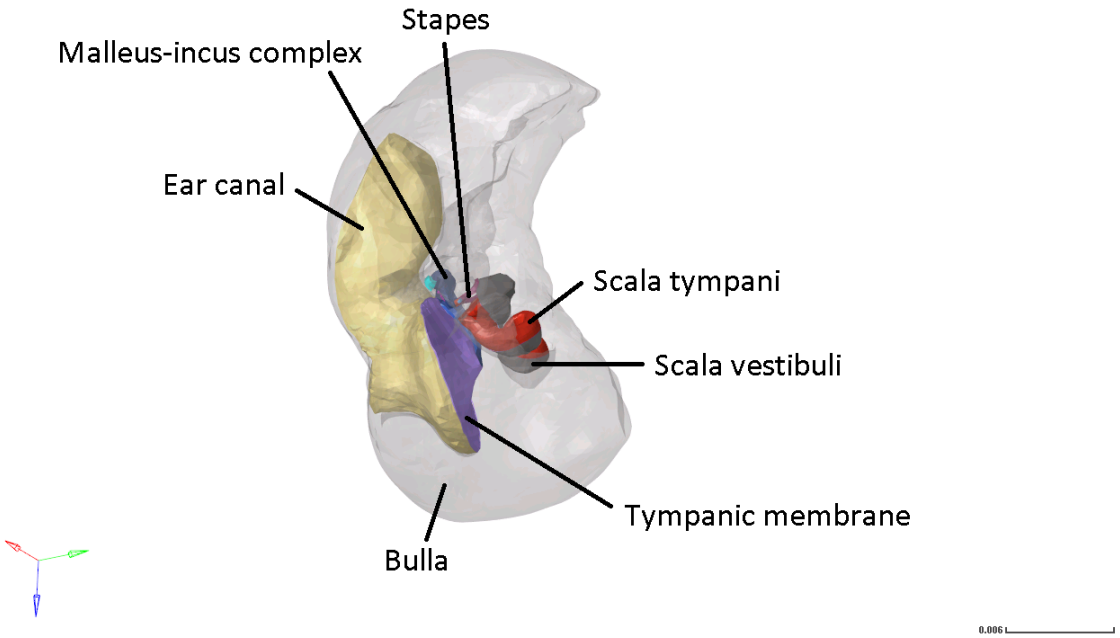

Figure 23. Posterior view of the 3D FE model of the chinchilla ear including the external ear canal. Note that the bulla is rendered transparent for ease of viewing. Scale bar is 0.006 m.

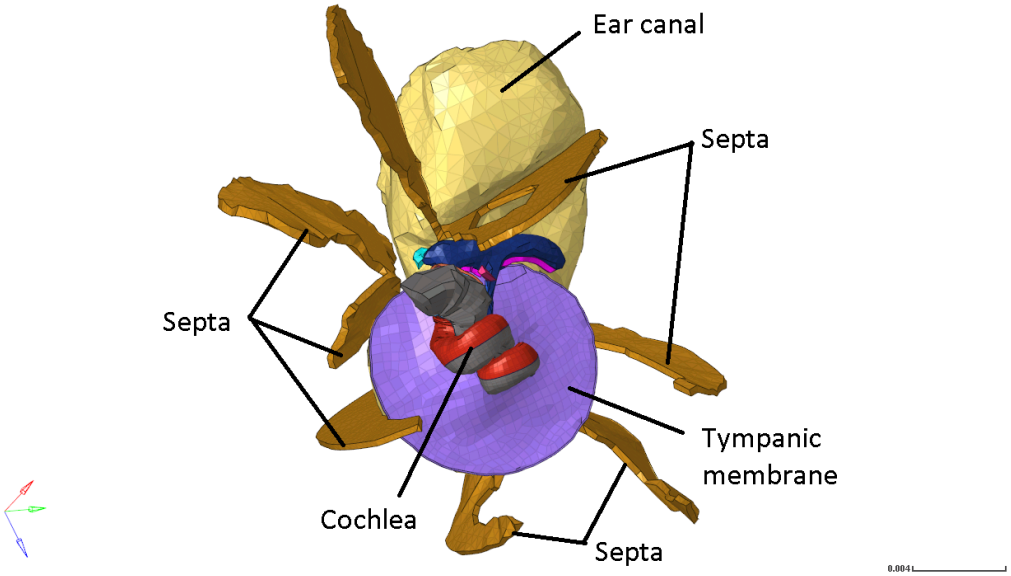

Figure 24. Medial view of the FE model of the chinchilla ear including the ear canal, TM, ossicular chain and supporting ligaments, septa, and cochlea. Bulla is excluded for viewing purposes. The scale bar is 0.004 m.

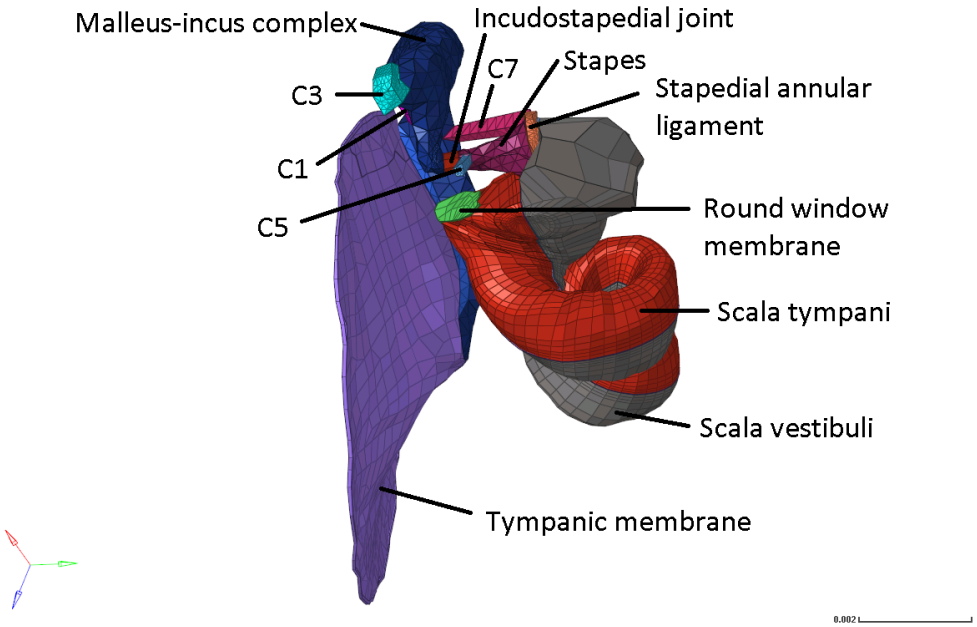

Figure 25. Posterior view of the middle ear structures and cochlea. The connection between the TM and cochlea through the ossicular chain is prominently displayed. Note the emphasis on suspensory ligaments. The scale bar is 0.002 m.

The whole FE model consisted of 234,919 elements and 75,885 nodes. The air fluid in the ear canal and bulla, as well as the liquid fluid in the cochlea were composed of FLUID30 elements. FLUID30 elements are 3D acoustic fluid elements used for modeling fluid medium and the interface in fluid/structure interaction problems. FLUID30 has four degrees of freedom: translations in the nodal x, y, and z directions, and pressure. This element type is particularly suited for applications in sound wave propagation (ANSYS Inc., 2013). The fluid in the ear canal were 4-node tetrahedral elements, while the fluid in the cochlea were 8-node hexahedral elements.

The septa, ossicular chain, and suspensory ligaments in the middle ear were modeled by 4-node tetrahedral elements (SOLID45), while the TM was modeled by 8-node hexahedral elements (SOLID45). The basilar membrane and bony supports of the cochlea were modeled by 8-node hexahedral elements (SOLID45). SOLID 45 elements have three degrees of freedom: translations in the nodal x, y, and z directions. This element type has large deflection and large strain capabilities (ANSYS Inc., 2007).

3.2 Generating Model for Harmonic Response Analysis

This section will provide a general overview of ANSYS Workbench before detailing the analysis system and briefly discussing the associated theories used in generating the 3D FE model of the entire chinchilla ear. The boundary conditions and material properties used in this acoustic simulation are also detailed.

3.2.1 ANSYS Workbench

Founded in the 1970s, ANSYS initially offered a single commercial general-purpose finite element program. Since then, it has become a giant in the engineering simulation industry, providing engineering simulation software that spans the entire range of physics. Currently, there are two primary ways to access the suite of ANSYS products. The first is through the original ANSYS environment, ANSYS Mechanical APDL (ANSYS Classic), which has a primitive graphical user interface (GUI) but primarily relies on the input of the ANSYS Parametric Design Language (APDL) commands. This is the platform that was used for the 2016 publication of the 3D FE model of the chinchilla middle ear. The second platform available is ANSYS Workbench, which consolidates ANSYS simulation products in a more user-friendly environment. All of the ANSYS, Inc. products can interface with each other in the Workbench environment. This platform still accepts APDL commands, but its drag-and-drop system modules and improved GUI allows the user to rely less on APDL code, facilitating the creation of analysis systems. The model presented in this thesis was generated in the ANSYS Workbench environment using harmonic response system analysis.

3.2.2 Structural Analysis in ANSYS Mechanical: Harmonic Response

Harmonic response analysis calculates the response of a system as a function of frequency. This type of analysis was used by Wang & Gan (2016) in characterizing middle ear functions using the 3D FE model of the chinchilla middle ear. Gan et al. (2007) also

used this analysis method to model sound transmission from the ear canal to the cochlea in a 3D FE model of the human ear.

Harmonic response analysis solves the general equation of motion for a structural system undergoing steady-state vibration **(1)**:

$$[M]\{\ddot{u}\} + [C]\{\dot{u}\} + [K]\{u\} = \{F^a\} \quad \textbf{(1)}$$

where [M] is structural mass matrix, [C] is the structural damping matrix, [K] is the structural stiffness matrix, {ü} is the nodal acceleration vector, {u̇} is the nodal velocity vector, {u} is the nodal displacement vector, and $\{F^a\}$ is the applied load vector (ANSYS Inc., 2009). The discretized structural mechanics equation models each finite element in the model, accounting for element shape, material properties, and boundary conditions, and are assembled into a larger system of equations that models the entire problem.

$$[M]\{\ddot{u}\} + [C]\{\dot{u}\} + [K]\{u\} = \{F^a\} \quad \textbf{(1)}$$

3.2.3 Equations Governing Acoustic Elements

The air in the ear canal and middle ear cavity, operating under the assumptions that air is compressible and inviscid with uniform mean pressure and density, were governed by the simplified lossless acoustic wave equation **(2)**:

$$\frac{1}{c^2}\left(\frac{\partial^2 P}{\delta t^2}\right) - \nabla^2 P = 0 \quad \textbf{(2)}$$

Where P is the acoustic pressure, c is the speed of sound ($\sqrt{k/\rho}$) in fluid medium, ρ is the mean fluid density, k is the bulk modulus of fluid, and t is time (ANSYS Inc., 2009; Gan

et al., 2007). The density and speed of sound of the air were assumed as 1.21 kg/m^3 and $^{346.1}$ m/s, respectively.

Equations 1 and **2** must be considered simultaneously in fluid-structure interaction problems. In the case of this model, there were fluid-structure interactions between acoustic elements that interfaced with movable structures such as the TM, ossicles, and basilar membrane.

3.2.4 ANSYS Harmonic Response Analysis Setup

The External Model component system was used to import the ".CDB" mesh file of the chinchilla ear into the ANSYS Workbench environment. The boundary conditions applied were based on those used by Wang & Gan, 2016. Briefly, the displacement boundaries of the TM annulus, stapedial annular ligament, and suspensory ligaments were fixed at the middle ear cavity wall. The bony support structures on either side of the basilar membrane were also assumed to be fixed.

The material properties used in the FE model of the chinchilla ear were adapted from literature. The mechanical properties of the middle ear structures were assumed as those used in Wang & Gan, 2016. Currently, no experimental data exists for the mechanical properties of the chinchilla basilar membrane from base to apex. However, studies in mice and gerbil have reported that stiffness of the basilar membrane generally decreases from base to apex (Emadi et al., 2004; Teudt & Richter, 2014). The Young's modulus of the basilar membrane in the FE human ear model (Gan et al., 2007) was assumed as 50 MPa at the base and linearly decreased to 15 MPa at the middle and further decreased to 3 MPa at the apex. The basilar membrane stiffness gradient assigned to the chinchilla model

reported in this thesis was 50 MPa at the base and 2.5 MPa at the apex. The β damping coefficient was 5 x 10^{-7} s at the base and increased to 0.3 x 10^{-3} s at the apex. The Young's modulus and damping coefficient β gradients are displayed in **Figure 26** and **Figure 27**, respectively.

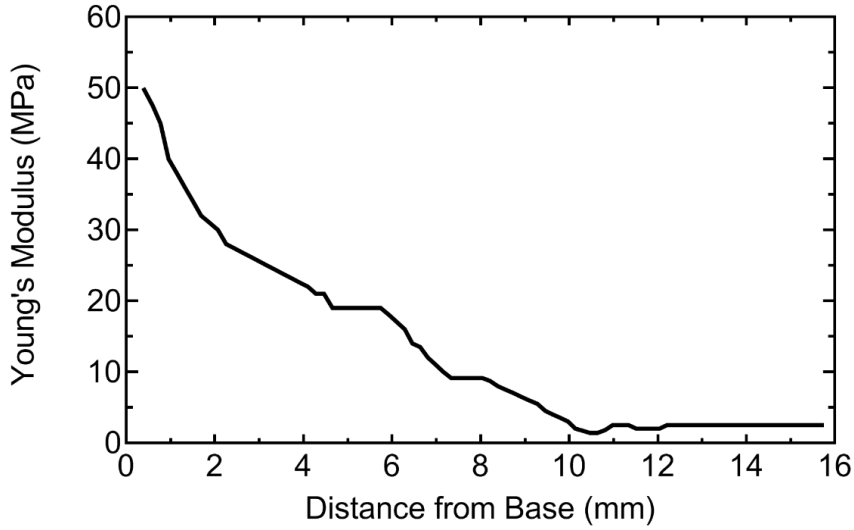

Figure 26. Young's modulus gradient from base to apex. The elastic modulus was 50 MPa at the base and decreased to 2.5 MPa at the apex.

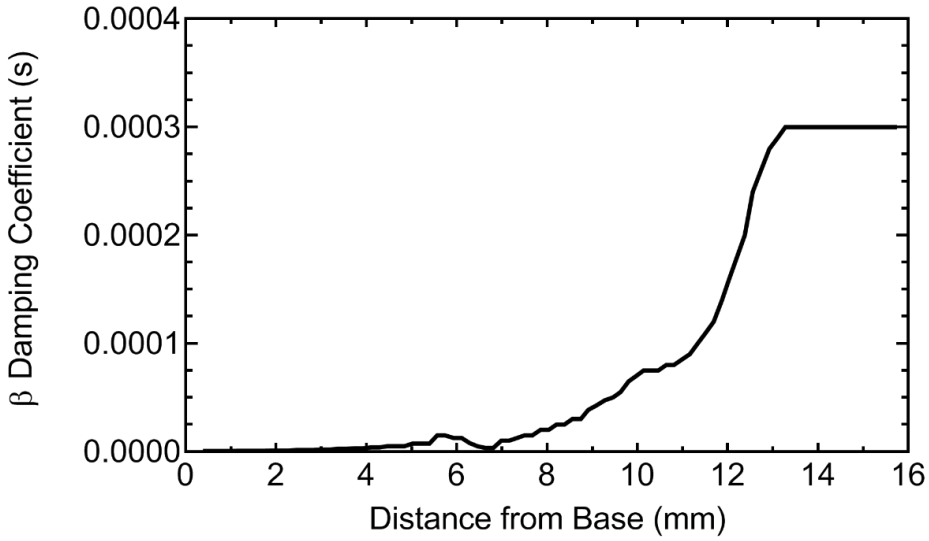

Figure 27. β damping coefficient gradient from base to apex. The β damping coefficient was 5 x 10^{-7} s at the base and increased to 0.3 x 10^{-3} s at the apex.

In order to model the air and cochlear fluid in the FE model, an Acoustics ACT Extensions was employed to define acoustics properties and apply acoustic boundary conditions and loads in mechanical without the need for APDL. The acoustic elements in the ear canal and middle ear cavity, as well as those in the cochlea, were designated as Acoustic Bodies. The density and sound speed of air were assumed as 1.21 kg/m^3 and 346.1 m/s, respectively. The cochlear fluid, known as perilymph, found in the scala vestibuli and scala tympani was modeled as a viscous, incompressible fluid with a density of 1,000 kg/m^3, sound speed of 1,500 m/s, and viscosity of 0.001 Pa·s. Fluid-structure interfaces (FSIs) where the acoustic pressure was coupled into structural analysis were defined in surfaces next to a movable structure (e.g. the TM, ossicles, basilar membrane, and RWM). Surfaces next to the ear canal wall and middle-ear cavity wall (both of which were fixed) were assigned an acoustic impedance value of 150,000 $Pa \cdot s/m^3$ and assumed to be fixed.

A sound pressure of 90 dB SPL (0.632 Pa) was applied in the ear canal at 2 mm away from the TM at the umbo. The displacements of the stapes FP and TM were determined from the harmonic response analysis over the auditory frequency range of 100 Hz to 15 kHz. The basilar membrane displacement from base to apex was also determined.

3.3 Results and Validation

The magnitude of the TM and stapes FP displacement in the direction normal to the FP was normalized by the input sound pressure (0.632 Pa). The TM displacement and stapes FP displacement were compared to the analysis results from the 3D FE Model of the chinchilla middle ear model (**Figure 28**). These results were also compared to experimentally derived data (**Figure 29**).

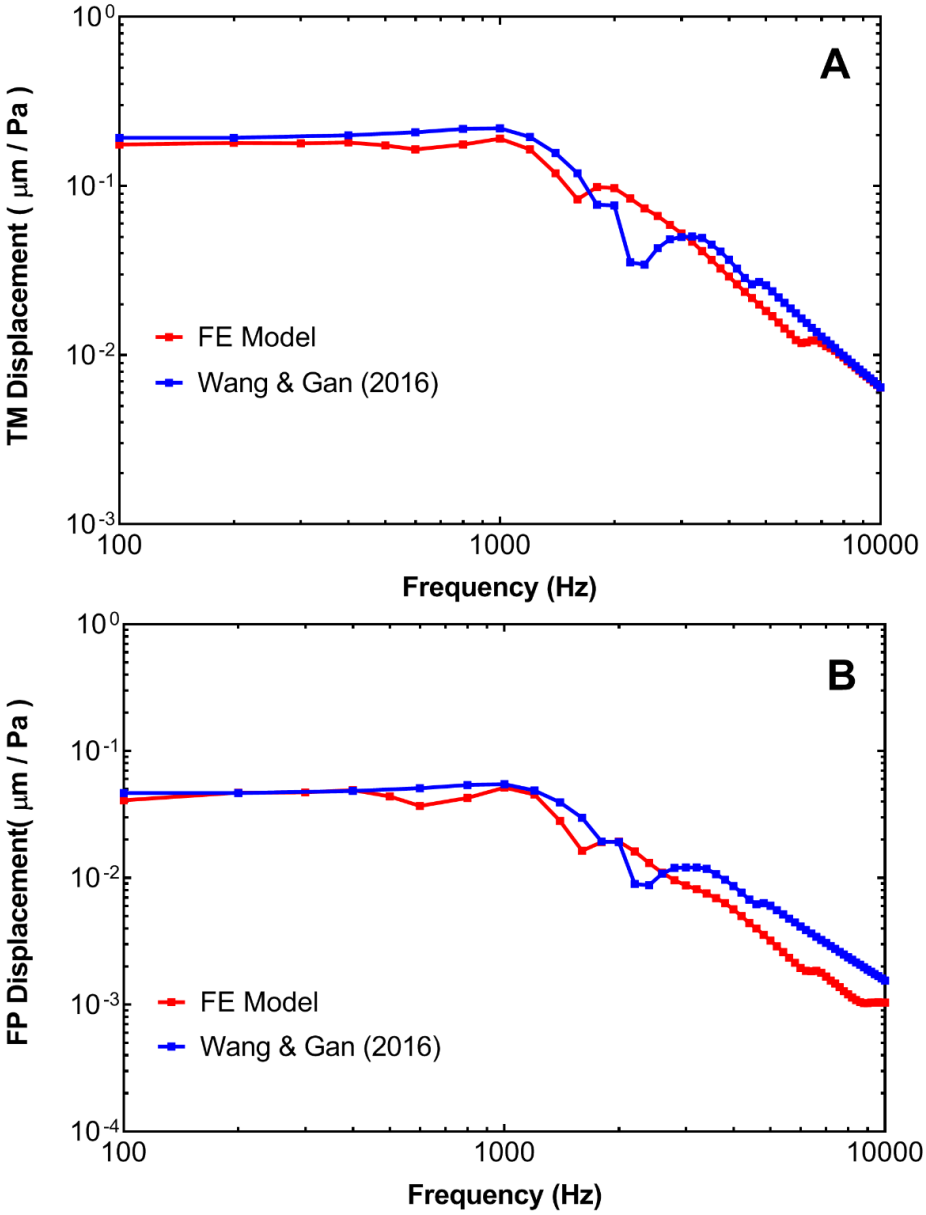

Figure 28. FE model derived displacements of the (A) TM at the umbo and (B) stapes FP in comparison to the published FE model of the chinchilla middle ear (Wang & Gan, 2016).

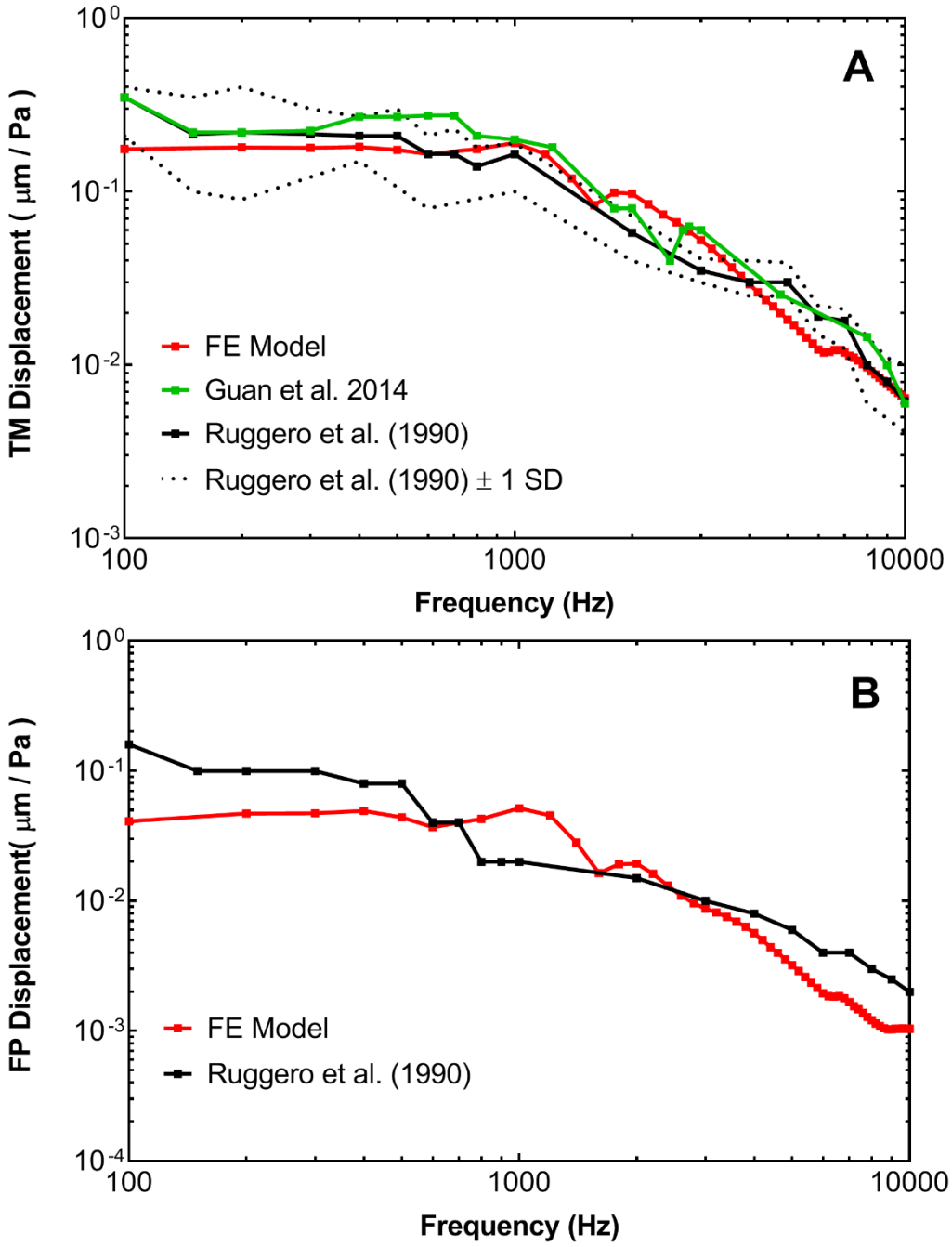

Figure 29. FE model-derived displacements of the (A) TM at the umbo and (B) stapes FP in comparison to published experimental data in chinchilla (Guan et al., 2014; Ruggero et al., 1990).

The displacement of the basilar membrane from the base to the apex over frequencies ranging from 200 Hz to 15 kHz were also derived (**Figure 30**). The basilar membrane displacement (d_{BM}) was normalized by the stapes FP displacement (d_{FP}) across the frequency range. This data was compared to the frequency versus position map created from published chinchilla experimental data (**Figure 31**) (Greenwood, 1990).

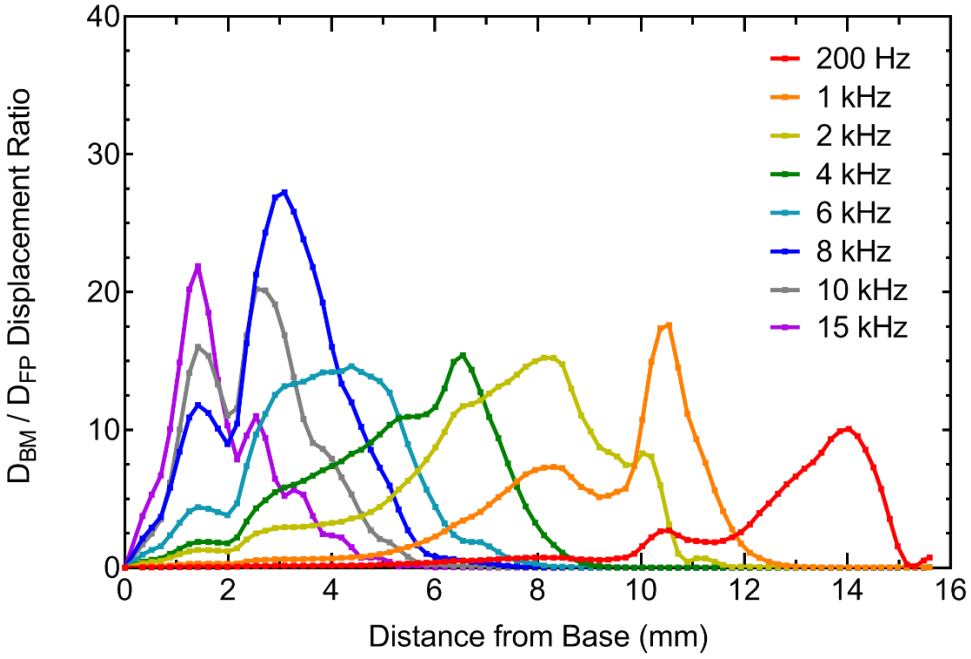

Figure 30. BM displacement normalized with respect to the footplate displacement (d_{BM} / d_{FP}) at frequencies of 200 Hz – 15 kHz from the base to apex.

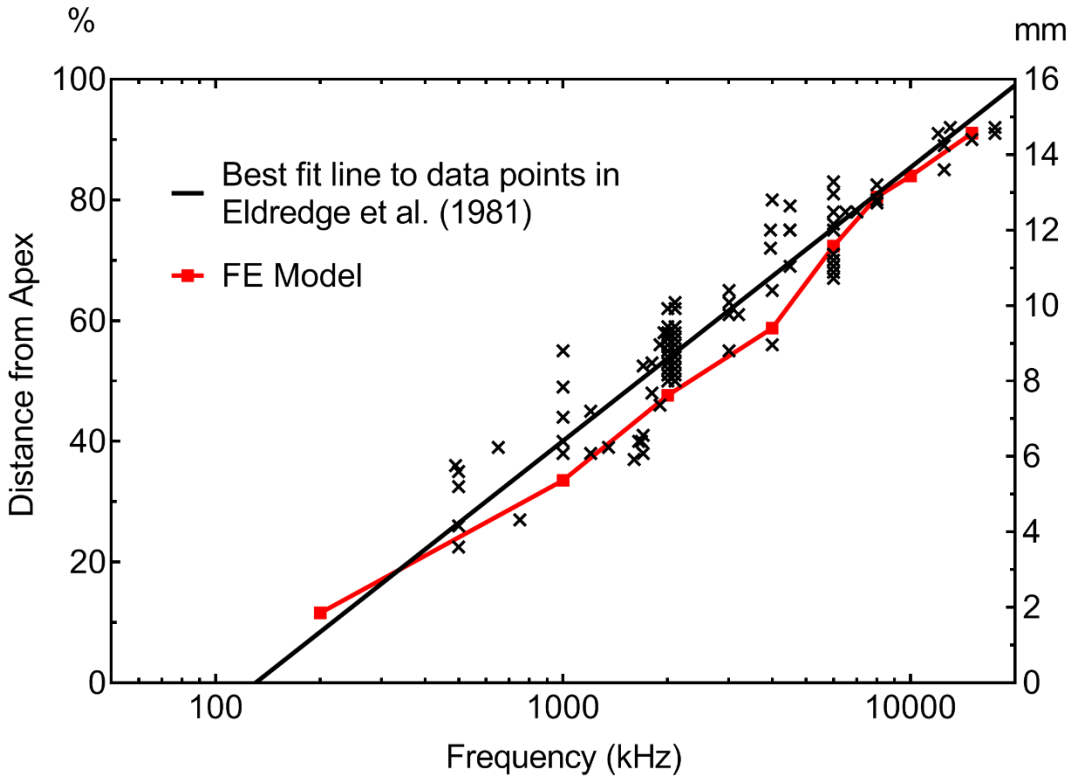

Figure 31. FE model-derived frequency versus position map in comparison to published chinchilla experimental data. The black line represents the line of best fit to data points (Eldredge et al., 1981).

As seen in **Figure 28A**, the TM displacement predicted by the FE model of the entire chinchilla ear was similar to that predicted by the model published by Wang & Gan (2016). The umbo displacement derived from this model was about 0.18 μm/Pa at low frequencies. While the predicted stapes FP displacement was similar to that predicted by the middle ear model at low frequencies, the FP displacement predicted by the whole ear model was relatively lower at frequencies of 2,800-10,000 Hz (see **Figure 28B**). The discrepancy may be due to the differences in how the cochlea was modeled. The mass block and dashpot system used by Wang & Gan (2016) simulated a cochlear impedance of

100 GW. The reduction in movement by the stapes at high frequencies suggests that the spiral cochlea in the FE model of the entire chinchilla ear had a greater impedance.

The TM displacement predicted by the FE model presented in this thesis generally agrees with the experimental data from chinchilla, as shown in **Figure 29A**. As shown in **Figure 29A**, the model-derived umbo displacement was about 0.18 μm/Pa at low frequencies, which was slightly lower than the experimental measurements. However, the TM displacement predicted by the model agreed with the experimental data collected by Ruggero et al., 1990, falling within ± 1 SD of the average TM displacement.

Figure 29B shows that the model-derived FP displacement follows the trend of experimental data collected by Ruggero et al. (1990). However, the FE model predicated FP displacement was relatively low in comparison at low and high frequencies. As noted by Wang & Gan (2016) this may be because the anatomical ossicular lever ratio, or the ratio between the length of the manubrium and length of the incus long process, was 3.76, which was larger than that of Ruggero's measurement of 2.94. However, the reported anatomical ossicular lever ratio ranges widely in literature, from 2.84 to 3.66 in chinchilla (Wang & Gan, 2016).

The normalized displacement of the basilar membrane along the longitudinal length of the BM from the base to apex shown in **Figure 30** indicates that lower frequencies peak closer to the apex (x = 16 mm) while higher frequencies peak closer to the base (x = 0 mm). The distribution of frequencies in this manner agrees with the well-established knowledge that the basilar membrane is organized tonotopically. Tonotopic organization of the basilar membrane provides mechanical tuning that provides the frequency sensitivity in the cochlea as reported by von Békésy on experimental measurements (Békésy, 1960).

In **Figure 31**, the FE model predicted basilar membrane displacement is compared to an experimentally derived frequency-position map for the chinchilla cochlea (Eldredge et al., 1981). In Eldredge et al., 1981, frequencies of tones were mapped on to locations along the organ of Corti. The locations were expressed as percentage distance from the apex of the cochlea, facilitating comparison of cochlea of different lengths. As seen in **Figure 31**, the FE model predicted frequency-position map agrees with that presented by Eldredge et al. At 200 Hz and 15 kHz, the FE model predicted that the traveling wave associated with this frequency (see **Figure 30**) would peak approximately at 12% and 91% from the apex, respectively. The FE model results deviated the most from the best fit line at 1 kHz, 2 kHz, and 4 kHz. However, Eldredge et al. noted that individual data points varied greatly and attributed to this variation to true differences among chinchilla ears (Eldredge et al., 1981).

3.4 Chapter Summary

A 3D FE model of the entire chinchilla ear, including the cochlea, was created. A uniform acoustic pressure was applied 2mm away from the TM and harmonic analysis was conducted using ANSYS Workbench to predict the displacements of the TM, stapes FP, and basilar membrane. FE model predicted results were then compared to experimental data to validate the model. Comparison of the FE model results and measurements taken from animal models demonstrated that the FE model could represent the main characteristics of TM displacement, and to a lesser degree stapes FP displacement, in chinchilla. Furthermore, the results of the FE model derived basilar membrane

displacement indicate that the model can capture the tonotopic distribution of the basilar membrane in the cochlea.

In summary, the first-ever 3D FE model of the entire chinchilla ear was created and used to simulate sound transmission from the ear canal to the cochlea.

Chapter 4: 3D FE Model of Chinchilla Ear for Blast Wave Transmission

As reported in Chapter 3, the FE model of the entire chinchilla ear, including the spiral cochlea, was created and used for acoustic analysis. However, the analysis technique used in this situation was a linear analysis, which calculated only the steady-state, linear response to an applied uniform acoustic pressure in the frequency domain. This technique does not adequately represent a blast overpressure waveform, nor the associated nonlinear effects. Therefore, a solver method more suitable for blast analysis was needed.

This chapter will focus on the adaptation of the newly developed FE model of the chinchilla ear for the analysis of blast wave transmission. A brief overview of the solver methodology utilized in Leckness et al. (2018) for blast wave analysis of the FE model of the human ear and its implementation regarding this model will be described. The boundary conditions and material properties ascribed to the model will be detailed. Finally**,** **preliminary** results and commentary on needed improvements will be provided.

4.1 Strongly Coupled FSI Analysis Scheme for Modeling Blast Wave Transmission

As mentioned previously, Leckness et al. (2018) reported the use of a strongly coupled FSI analysis method to computationally model blast wave transmission through the human ear. This method can be found in Leckness' MS thesis (2016) and utilizes the ability of ANSYS to conduct multiphysics analyses to simulate the interaction between fluid flow and structural mechanics that occurs during blast wave propagation. FLUENT and ANSYS Mechanical (Transient Structural) analysis systems were used to solve the fluid and structural domains, respectively (Leckness, 2016). As in Leckness (2016), the

fluid domains of this model consisted of the air in the ear canal and middle ear cavity. However, the inclusion of the spiral cochlea of this model, which was absent in Leckness' model of the human ear, necessitated the inclusion of the cochlea in the fluid domain as well. Likewise, the structural domain of this model was similar to Leckness' model, including the TM, TMA, ossicular chain and associated suspensory ligaments. However, the RWM and the basilar membrane and its associated bony supports were also included in the structural domain of this model, unlike that of Leckness'.

In order to accurately simulate the two-way fluid-structure interaction that occurs during blast wave transmission through the ear, computational fluid dynamics and structural mechanics must be co-simulated. Tightly integrated coupling of FLUENT and ANSYS Mechanical was achieved by system coupling the two analysis systems in the ANSYS Workbench user environment (Leckness, 2016). The simulation of the two-way fluid-structure interaction is especially important for modeling blast wave transmission through the chinchilla ear due to the large volume of air found in the large middle ear cavity of chinchilla. **Figure 32** below shows the project schematic of the system coupled analysis systems as it pertains to the model of the chinchilla ear. The ".CBD" structural mesh file, which included the structural domain, were imported into ANSYS Mechanical while the .MSH files containing the fluid domains were transferred into FLUENT.

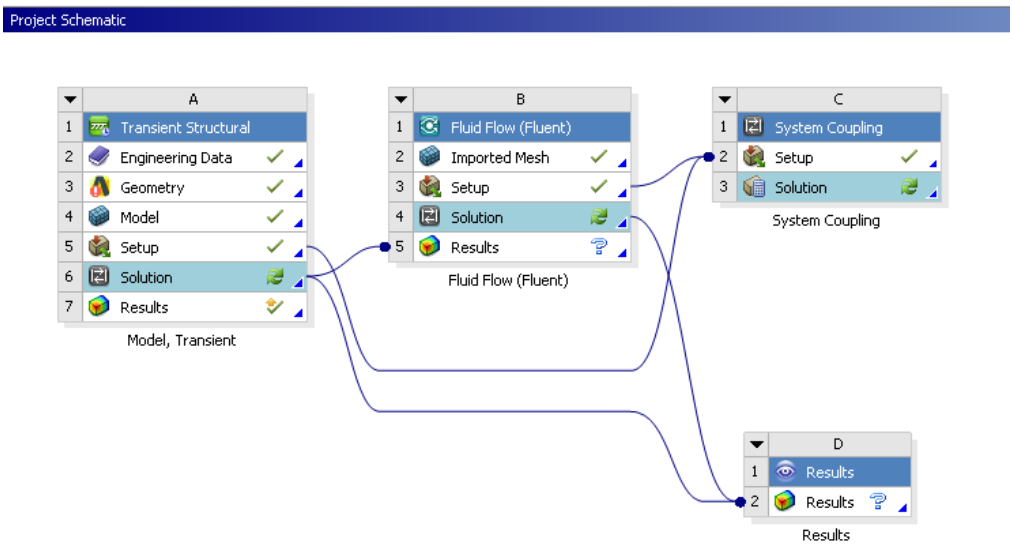

Figure 32. ANSYS Workbench project schematic showing data flow from FLUENT and ANSYS Mechanical (Transient Structural) to system coupling.

The two-way communication between FLUENT and ANSYS Mechanical is achieved through the Workbench component system, System Coupling, which handles data transfers that occur bi-directionally between the analysis systems. These data transfers are determined by the application of FSIs which the user specifies on mesh faces that coincide in both FLUENT and ANSYS Mechanical. For example, the interface of the basilar membrane with the fluid in the cochlea and the interface of the fluid in the cochlea with the basilar membrane were both designated as FSIs. The coupling service and participant solvers advance synchronously through a coupled analysis. The execution sequence of the System Coupling service controlling the analysis is described in depth in Leckness (2016) and, for the sake of brevity, will not be discussed herein. Furthermore, a detailed discussion of the solver tactics of FLUENT will not be included in this thesis, as they are similar to those reported in Leckness (2016). The solver tactics of ANSYS Mechanical have been previously discussed in Chapter 3.

4.2 Generating the Model for Blast Wave Simulation

This section will focus on the analysis setups for FLUENT and ANSYS Mechanical, namely the applied loads and boundary conditions that were used to represent the physics of blast wave transmission through the chinchilla ear.

4.2.1 Fluid Analysis Setup

The analysis in FLUENT was set up for transient, compressible, laminar fluid flow. Fluids are classified as incompressible and compressible, where compressible fluids undergo significant changes in density as they flow while incompressible fluids do not. Generally, compressibility effects are considered significant if the Mach number, or the speed of an object in relation to the speed of sound, is greater than 0.3. A blast wave, which consists of a shock wave and blast wind (Stuhmiller et al., 1991), creates a sharp change in pressure level and necessitates the consideration of compressibility effects. Moreover, the velocity of a shock wave is supersonic compared to the local sound speed in the surrounding medium. For these reasons, compressibility was considered in this analysis. Laminar flow was selected as the flow regime because the high velocity pressure front that enters the ear canal quickly loses velocity at the end of the canal, where the total pressure measured is primarily static pressure (Leckness, 2016).

Standard compressible air properties were used for the fluid in the ear canal and middle ear cavity. The fluid in the cochlea was modeled as liquid water. The operating pressure was assumed as ambient air pressure at sea level (101,325 Pa) and the effects of gravity were neglected. A recorded BOP waveform from a chinchilla animal test was applied as an input at the entrance of the ear canal, which was defined as a pressure-inlet

(**Figure 33**). The walls of the ear canal, middle ear cavity, and cochlea were defined as rigid, no slip walls.

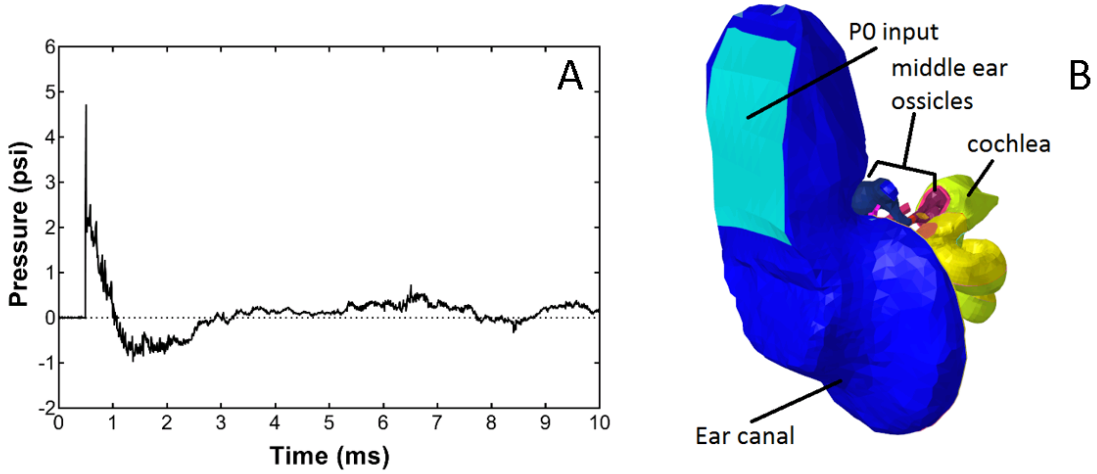

Figure 33. (A) A recorded BOP waveform at the entrance of the ear canal from an animal test with a peak pressure of 4.7 psi. (B) Model image with the entrance of the ear canal in light blue. The waveform was applied at the entrance of the ear canal in the model in FLUENT to drive the analysis.

The high pressure caused large deformation of the TM, which in turn led to large deformation of the FSIs in the model. Thus, the dynamic smoothing and remeshing scheme employed by Leckness (2016) was also used in this model to maintain a level of cell quality sufficient for convergence under conditions of large deformation.

FSIs on either side of the TM, RWM, and BM were applied to transfer the fluid forces acting on these structures into these structures in ANSYS Mechanical and in turn to receive the structural displacements. An FSI on the stapes FP was also created to capture the interaction occurring where the stapes terminates at the cochlea. The fluid-structure interaction between the ossicular chain and air in the middle ear cavity was assumed negligible (Leckness, 2016).

There are four pressure-velocity coupling algorithms that may be used to calculate a solution: SIMPLE, SIMPLEC (SIMPLE-Consistent), PISO (Pressure-Implicit with Splitting of Operators) and COUPLED. Segregated solvers such as PISO, SIMPLE, and SIMPLEC are advantageous for large cases in which direct-coupled solvers (e.g. COUPLED) become unaffordable due to large resource-demands. PISO is similar to the SIMPLE and SIMPLEC algorithms but can drastically reduce the number of iterations needed for convergence, particularly for transient problems. PISO also has the advantage of reducing convergence difficulties associated with highly distorted meshes. For these reasons, PISO was utilized as the pressure-velocity coupling algorithm for this analysis.

The analysis duration was set to 4 ms with a time step size of 1 μs. Static pressure monitors were initialized at locations of interest to determine the predicted pressure waveforms. The locations of interest included in front of the TM in the ear canal (P1) and behind the TM in the middle ear cavity (P2), as shown in **Figure 34**. The pressure in the cochlea along its spiral were also desired. Pressure monitors at three locations within the scala vestibuli (SV-1, SV-2, and SV-3) and scala tympani (ST-1, ST-2, and ST-3) each were used to determine the pressure distribution within the cochlea. SV-1 was located approximately 0.6 mm below the stapes FP, while SV-2 and SV-3 were located about 5 mm and 13 mm from the base, respectively. ST-1 was located roughly 0.9 mm below the RWM, while ST-2 and ST-3 were located approximately 6 mm and 13 mm from the base, respectively. The locations of the pressure monitors in the scala vestibuli and scala tympani are shown in **Figure 35**.

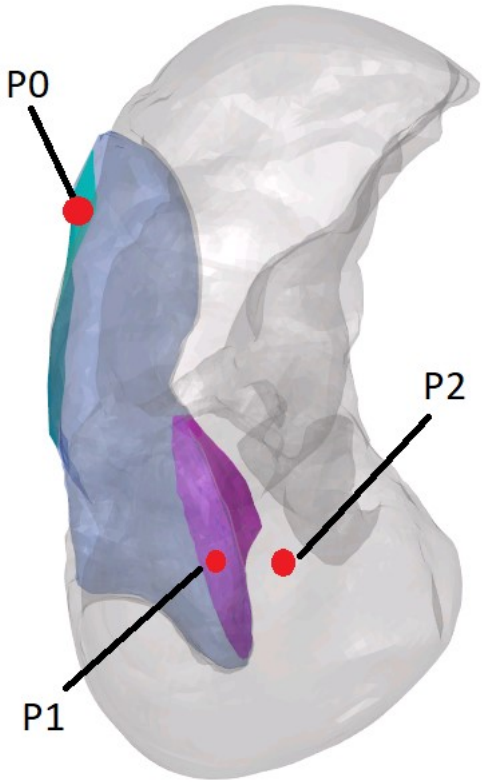

Figure 34. Locations of P0, P1, and P2 pressure calculated in the ear canal and middle ear cavity. P1 was located approximately 2 mm lateral to the TM. P2 was located approximately 1.5 mm medial to the TM. The cochlea has been removed for ease of viewing.

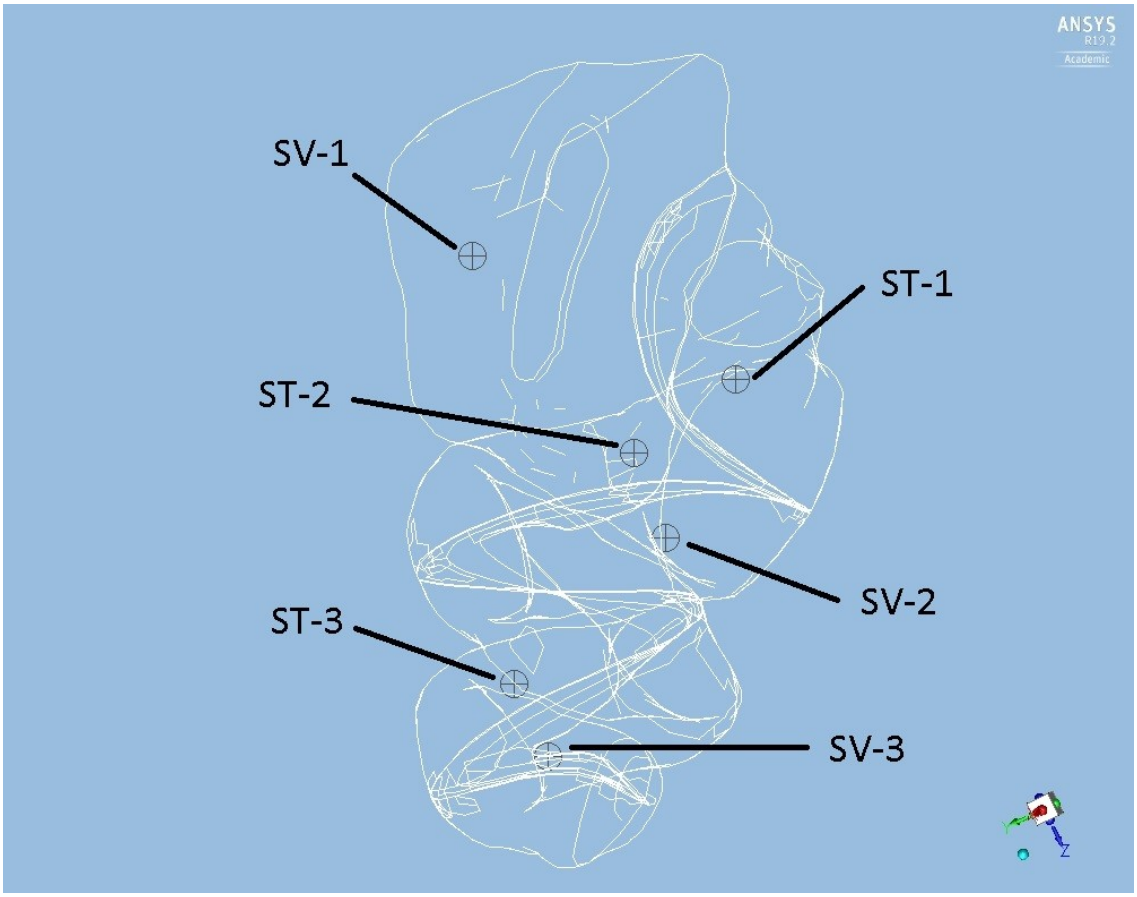

Figure 35. Locations of the pressure calculated in the scala vestibuli (SV-1, SV-2, and SV-3) and scala tympani (ST-1, ST-2, and ST-3). The outlines of the scala vestibuli, scala tympani, basilar membrane, and supporting bony structures in the cochlea are shown for context and ease of viewing.

4.2.2 ANSYS Mechanical Analysis Setup

The structural components of the chinchilla ear including the TM, TM annulus, ossicular chain and associated suspensory ligaments, septa, and basilar membrane and supporting bony structure were imported in ANSYS Mechanical. The material properties of these structures in the middle ear were based on those used in Wang & Gan (2016), though there did exist slight differences. Notably, the elastic modulus of the TM was decreased to 150 MPa and the damping coefficient of some structures were reduced. The

Poisson's ratio of all solid structures was assumed as 0.3. The material properties used for middle ear structures in this model are listed in **Table 1** below. The material properties of the basilar membrane were assumed as those reported in Chapter 3.

Table 1: Material properties of chinchilla ear model for blast wave analysis

Structure	Parameters
Tympanic membrane	
Elastic modulus (MPa): Pars tensa	150
Pars flaccida	15
Density (kg/m^3)	1100
Damping coefficient	
Pars tensa	1.0×10^{-6}
Pars flaccida	7.5×10^{-5}
Manubrium	
Elastic modulus (MPa)	800
Density (kg/m^3)	1000
Damping coefficient	7.5×10^{-5}
Incudostapedial (IS) joint	
Elastic modulus (MPa)	10
Density (kg/m^3)	1000
Damping coefficient	7.5×10^{-5}
Stapedial annular ligament (SAL)	
Elastic modulus (MPa)	0.12
Density (kg/m^3)	1200
Damping coefficient	1.25×10^{-4}
Anterior malleal ligament (C1)	
Elastic modulus (MPa)	3.2
Density (kg/m^3)	1000
Damping coefficient	1×10^{-6}
Posterior incudal ligament (C3)	
Elastic modulus (MPa)	2.5
Density (kg/m^3)	1000
Damping coefficient	7.5×10^{-5}
Posterior stapedial tendon (C5)	
Elastic modulus (MPa)	1.2
Density (kg/m^3)	1000
Damping coefficient	7.5×10^{-5}
Tensor tympani tendon (C7)	
Elastic modulus (MPa)	2.0
Density (kg/m^3)	1000
Damping coefficient	7.5×10^{-6}
Malleus-incus complex	

Elastic modulus (GPa)	14.1
Density (kg/m^3)	2000
Damping coefficient	7.5 x 10^{-5}
Stapes	
Elastic modulus (GPa)	14.1
Density (kg/m^3)	1500
Damping coefficient	5 x 10^{-5}
RWM	
Elastic modulus (MPa)	0.2
Density (kg/m^3)	1000
Damping coefficient	5 x 10^{-5}

The TM annulus and regions where the ligaments meet the bony structure of the middle ear cavity were set as fixed boundary conditions. The bony support structures on either side of the basilar membrane were also assumed to be fixed. FSIs on either side of the TM, RWM, and basilar membrane, as well as at the interface between the stapes FP and scala vestibuli, were established to model the fluid-structure interactions that occur. The initial displacement of the structures in the middle ear is driven by the pressure input the TM receives from FLUENT via the data transfer managed by System Coupling.

The displacements of the TM, stapes FP, and basilar membrane were key outputs from ANSYS Mechanical. In particular, the movement of the basilar membrane were of interest because its movement under blast conditions is not well studied and because displacement of the basilar membrane may be useful in predicting damage to the inner ear.

4.3 Results

The preliminary results from the FE model of the chinchilla ear for blast wave analysis are shown in this section. Few experimental results in chinchilla exist in literature to compare with the model predicted values. However, representative experimental BOP

waveforms recorded at the entrance of the chinchilla ear canal (P0) and near the TM in the canal (P1) exist and provide guidance in evaluating the current model (**Figure 36**).

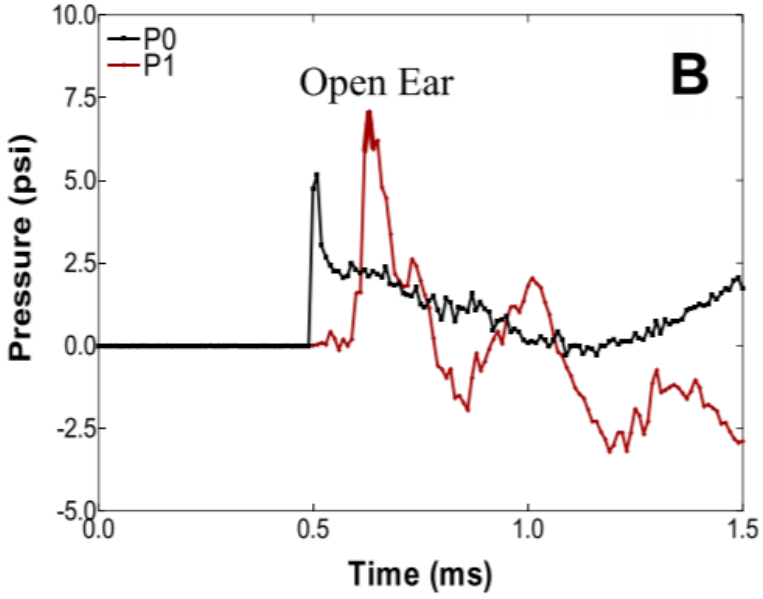

Figure 36. Representative waveforms recorded at the entrance of the ear canal (P0) and near the TM in the canal (P1) from chinchilla animal model used in blast exposure study (Chen et al., 2019).

As seen in **Figure 36**, the reported P1 peak pressure was greater than the P0 peak pressure, which was due to the amplification function of the outer ear. In comparison to the experimental waveforms, the model-predicted P0, P1, and P2 waveforms do not follow the trend shown in **Figure 36**. While experimental measurements indicate that the P1 peak pressure should be greater than the P0 peak pressure, the model-derived results demonstrated the opposite (**Figure 37**). Instead, the P1 peak pressure at 3.9 psi was less than the P0 peak pressure at 4.7 psi.

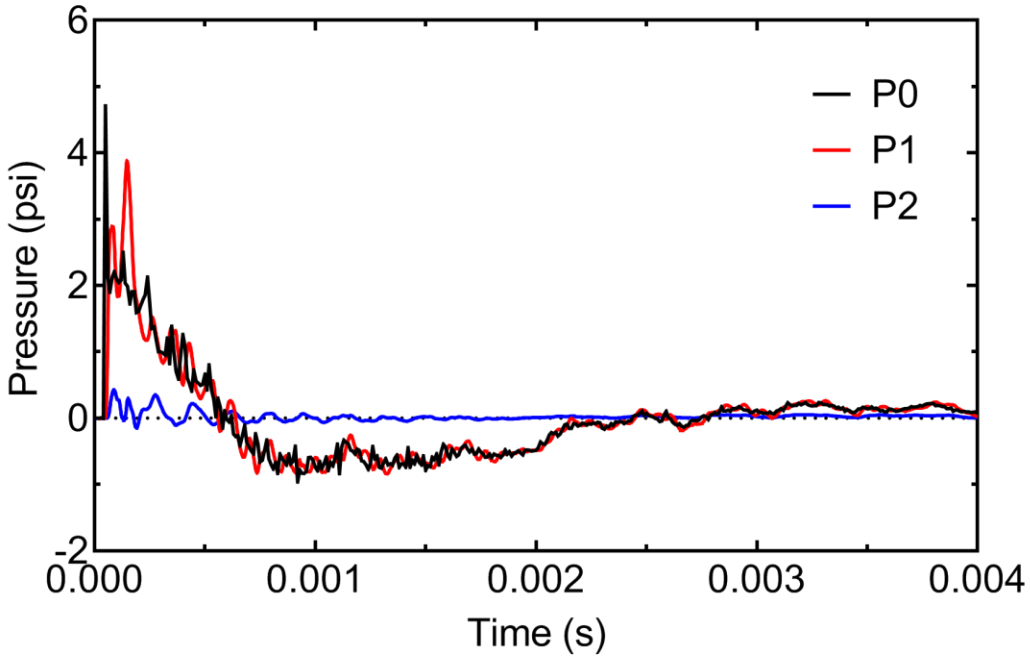

Figure 37. FE model-predicted pressure waveforms at the entrance of the ear canal (P0), in front of the TM in the canal (P1), and behind the TM in the middle ear cavity (P2). Note that the peak P0 pressure was 4.7 psi, while the peak P1 pressure was 3.9 psi.

In addition to the pressure measurements predicted in the canal and middle ear cavity, the pressure distribution in the cochlea was also predicted. **Figure 38** shows the calculated pressure waveforms at different locations in the cochlea. As mentioned previously, SV-1 was located approximately 0.6 mm below the stapes FP, while SV-2 and SV-3 were located about 5 mm and 13 mm from the base, respectively. ST-1 was located roughly 0.9 mm below the RWM, while ST-2 and ST-3 were located approximately 6 mm and 13 mm from the base, respectively.

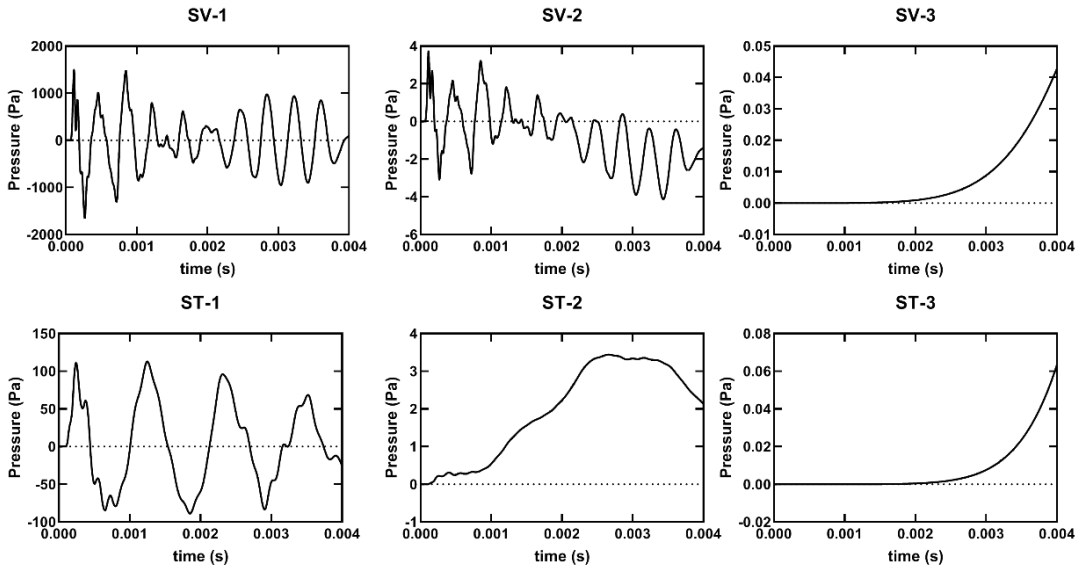

Figure 38. FE model-derived pressures in the cochlea in response to BOP input. Pressure was calculated at three different points in the scala vestibuli (SV) and scala tympani (ST) each. Note that the pressure was greatest in the SV near the footplate (SV-1) but decreased closer to the helicotrema (SV-3) and into the ST.

The results shown in **Figure 38** demonstrate that the pressure closest to the stapes in the scala vestibuli (SV-1) was the greatest, with a maximum peak pressure of approximately 1,500 Pa. As the location moved closer to the helicotrema, the pressure in the scala vestibuli decreased. SV-2 and SV-3 had maximum peak pressures of 3.7 Pa and 0.04 Pa, respectively. In the scala tympani, the model-predicted pressure was greatest near the RWM, with a maximum peak pressure of about 113 Pa. Similar to the trend observed in the scala vestibuli, as the location moved closer to the helicotrema the pressure in the scala tympani decreased. ST-2 and ST-3 had peak pressures of 3.4 Pa and 0.06 Pa. These results indicated that the pressure wave in the cochlea did not distribute to the apex but had decreased substantially less than halfway down the cochlea.

The displacements of the TM and stapes FP were also predicted by the model in response to BOP and are shown in **Figure 39** below. The maximum displacement of the TM was 1.05 mm. The initial positive displacement value of the TM umbo indicates that the TM displaced into the middle ear cavity for roughly the first 0.0005 s. The following negative displacement reflects TM movement into the ear canal, which lasted until about 0.003 s. TM movement was minimal for the remaining time.

The peak-to-peak displacement of the stapes FP was approximately 12 μm. The stapes FP displacement over time demonstrates that the FP displaced in towards the cochlea before moving back into the middle ear cavity and then briefly into the cochlea again.

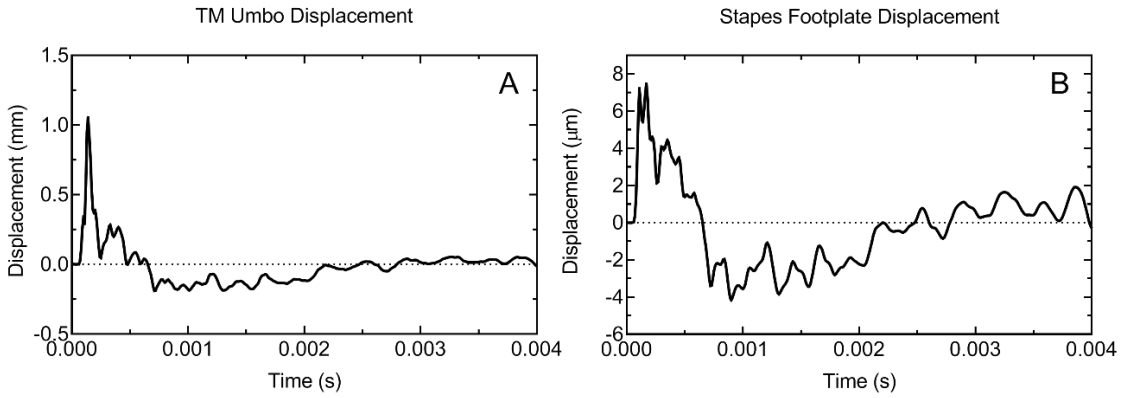

Figure 39. Model-predicted displacements of the (A) TM at the umbo and (B) stapes footplate in the normal direction in response to BOP input.

Finally, the displacements of the basilar membrane at 17 points from the base (near the stapes) to the apex (near the helicotrema) were predicted (**Figure 40**). The displacements were calculated in the direction normal to the basilar membrane. Positive displacements were established as movement into the scala tympani, while negative displacements reflected movement into the scala vestibuli. As movement of the basilar membrane in the direction of the scala vestibuli is associated with moving the hair cells

closer to the tectorial membrane (and thus can cause damage to the hair cells), displacement in the negative direction is the focus of this discussion.

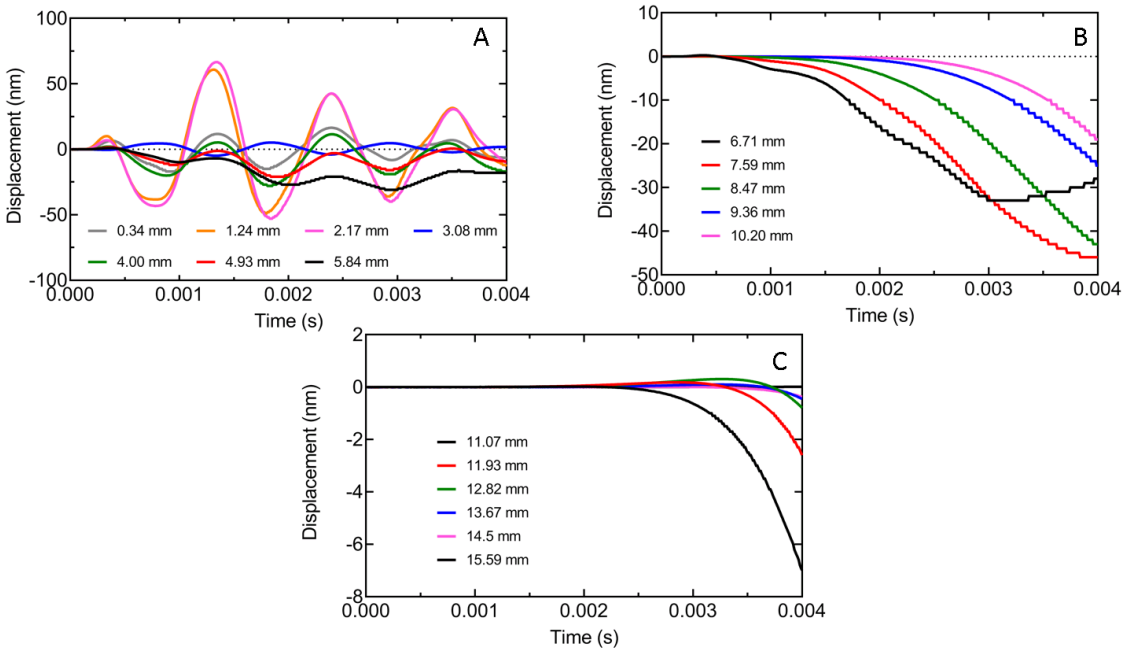

Figure 40. Basilar membrane displacement from base to apex in response to BOP in the time domain. (A) Displacements of the basilar membrane up to 5.84 mm from the base. (B) Displacements of the basilar membrane from 6.71 mm to 10.20 mm from the base. (C) Displacements of the basilar membrane from 11.07 mm to 15.59 mm from the base.

As seen in **Figure 40A**, the greatest basilar membrane displacement occurred 2.17 mm from the base with a maximum negative displacement of approximately 53 nm. The basilar membrane displayed an oscillating pattern of movement along the first 5.84 mm of length (**Figure 40A**). The displacement of the basilar membrane decreased from base to apex. After the first 5.84 mm, the basilar membrane movement showed displacement only in the negative direction or in the direction of the scala vestibuli (**Figures 40B-C**). Displacements close to the base started close to the time of blast and lasted throughout the duration of the simulation (**Figure 40A**). Though displacements in the middle section of the basilar membrane (**Figure 40B**) began slightly after those closest to the base, they also

continued for the duration of the simulation. However, the locations closest to the apex (**Figure 40C**) were not displaced until the latter half of the simulation.

4.3.1 Discussion

Experimentally recorded pressure waveforms in the chinchilla ear at the P0 and P1 locations indicated that the P1 peak pressure was greater than that of P0. Knowledge of these waveforms is useful in understanding damage to the TM caused by P1, and thus are important outputs of the FE model in simulating blast wave transmission. However, the results predicted by the FE model did not agree with the experimental measurements. An explanation for this discrepancy may be related to how the input pressure is applied in this model. The pressure in this model was applied normal to the surface designated as the inlet surface, which was the method used by Leckness (2016) for the FE model of the human ear for blast wave analysis. However, the human ear canal anatomy is different from the chinchilla ear canal anatomy. While the human ear canal from the opening to the TM is straight, the chinchilla ear canal runs dorsal-ventral (i.e., there is a 90° turn in the ear canal connecting to the TM). The pinna of the chinchilla serves to funnel sound into the ear canal, which may provide some directionality to the incoming pressure wave. Thus, applying the input pressure such that it has some degree of directionality may serve to mimic the function of the pinna and improve the results. Another method to improve the results is to simplify the problem by applying the P0 pressure closer to the TM in the ear canal, bypassing the 90° turn.

Though the TM and stapes FP displacements in response to BOP has yet to be experimentally measured in chinchilla, Jiang et al. (2019) recently reported dual-laser

measurement of human TM motion under blast exposure. This study used a BOP waveform with a peak pressure of about 5 psi, similar to that used in this simulation (Jiang et al., 2019). While exact TM displacement measurements may differ due to species differences, comparison of the overall trend may be useful. In Jiang et al. (2019), the TM started moving in response to BOP and then vibrated at an amplitude of 0.4 mm for about two cycles with a waveform similar to a sine wave before diminishing in amplitude after 2 ms. The chinchilla model-predicted TM displacement did not follow this trend. Instead, of oscillating in a sine wave like pattern, the TM reached peak positive amplitude and diminished quickly. As the TM and stapes are connected via the ossicular chain, the stapes FP predicted displacement also followed this pattern to a degree. The predicted movement of the stapes in response to BOP also differed from what was expected. With a peak pressure of about 184 dB SPL used as the input for this model, the predicted stapes movement is lower than what is reasonable.

The pressure in the cochlea is driven by the stapes movement. The model-predicted pressures in the scala vestibuli and scala tympani revealed that the greatest pressure occurred in the scala vestibuli near the base, which is reasonable considering that this location is nearest the stapes FP. However, examination of locations closer to the apex indicated that the pressure waveform did not travel far from the base, but instead diminished about halfway down the cochlea. At the location nearest the helicotrema (ST-3 and SV-3 located about 13 mm from the base), the pressures in the scala vestibuli and scala tympani were approximately equal (0.04 Pa and 0.06 Pa, respectively). The basilar membrane displacement at 12.82 mm was close to zero nm, reflecting the role that the pressure gradient in the cochlea has on basilar membrane displacement.

While the displacement of the chinchilla basilar membrane in response to blast exposure has yet to be determined experimentally, studies on basilar membrane displacement at different frequencies at lower dB SPL do exist in the literature. A 2011 study reported gerbil basilar membrane displacement ranging from 0.01-10 nm in response to 10-90 dB SPL stimulus (Ren et al., 2011). In a study on basilar membrane mechanics in the 6-9 kHz region of chinchilla cochleae, Rhode (2007) noted that the BM operating range in sensitive cochleae is 1-200 nm for intensities less than 100 dB SPL. It was also suggested that 1 μm displacement would be sufficient to cause hair cell damage (Rhode, 2007). The model-predicted basilar membrane displacement from base to apex in the direction of the scala vestibule (negative displacement) was greatest at 2.17 mm from the base, with a displacement of 53 nm. However, this displacement is not large enough to reflect the hearing damage observed in chinchilla animal models after blast exposure. Instead, the basilar membrane displacement predicted by the model fell within the range reported by literature on basilar membrane displacement in response to low dB SPL stimulus.

It should be emphasized that the findings presented above are the preliminary results from the FE model of the chinchilla ear for blast wave analysis. The current model requires many improvements in order to obtain more accurate results. However, this model represents a step towards understanding the transmission of BOP from ear canal to cochlea in the chinchilla ear, which may improve our understanding of hearing damage incurred by BOP.

4.4 Chapter Summary

FE analysis is a powerful tool that helps explain experimental observations or permits the simulation of experiments otherwise impossible. This thesis reported the

creation of a FE model of the chinchilla ear for blast wave analysis. **Preliminary** results consisting of the pressures in the ear canal, middle ear cavity, and cochlea in response to BOP were calculated. The TM, stapes, and basilar membrane displacements in response to BOP were also predicted. However, preliminary results indicated that the model needs to improve. Future work on the chinchilla FE model must continue, which were briefly touched on above and will be discussed further in Chapter 5.

In the context of this thesis, a FE model of the chinchilla ear to analyze blast wave transmission is desirable to augment chinchilla animal studies focused on the effects of blast exposure on hearing loss. Furthermore, such a model may facilitate the translation of experimental data between animal model of chinchilla and human. The model presented herein represents a starting point towards achieving these goals.

Chapter 5: Conclusion

5.1 Research Summary

There is an obvious need to fully understand the effects of blast exposure on auditory dysfunction and the mechanisms by which it occurs. Towards this goal, this thesis reports investigation of blast exposure in chinchilla animal model and a computational model of the entire chinchilla ear.

In the experimental study, chinchillas with and without earplugs were exposed to repeated low-intensity BOP. Function tests reflecting the state of the auditory system were recorded over a 14 day time period. The main findings of this study were that exposure to 6 repeated low-intensity blasts induced permanent hearing damage in both protected and unprotected ears, indicating that the protective function of HPDs was limited in this situation. Furthermore, hearing function changes showed damage in both the peripheral and central auditory systems. Finally, comparison with experimental measurements from a similar study in which chinchilla were exposed to 3 repeated low-intensity blasts demonstrated that 6 repeated blasts resulted in greater hearing loss.

To provide a comprehensive understanding of blast wave transmission, a FE model of the chinchilla ear for blast wave analysis was desired. However, current literature reported only a FE model of the chinchilla middle ear that simulated the cochlea using a mass block and dashpot system (Wang & Gan, 2016). As the inner ear is highly vulnerable to blast damage, a FE model of the cochlea reflecting the actual anatomy was needed. Thus, a FE model of the entire chinchilla ear including the spiral cochlea was developed. Harmonic response analysis was conducted to predict structural displacements in response to acoustic stimulus. Comparison of the model-predicted displacements and experimental

measurements validated the model. The model was able to predict the TM, stapes, and basilar membrane movement in response to an acoustic input.

The newly created FE model of the entire chinchilla ear was then modified for blast wave analysis. Generation of this model was based on the methods reported in Leckness' MS thesis (2016) for modeling blast wave transmission in a FE model of the human ear. Outputs from blast wave analysis in the FE model of the chinchilla ear included pressures in the ear canal, middle ear cavity, and cochlea, and structural displacements of the TM, stapes FP, and basilar membrane in response to BOP. Preliminary results indicated that the current model analysis needs to improve for simulating blast wave transmission from the ear canal to cochlea.

5.2 Future Work

Future studies using chinchilla animal models are needed to improve our understanding of blast-induced hearing loss. Further investigation of key blast parameters such as number of blasts, frequency of occurrence, blast intensity, and recovery time may provide more insight. Isolation of the PAS and CAS may also clarify the effect of repeated blast on the CAS. Knowledge gained from these studies may help in the prevention, diagnosis, and treatment of auditory dysfunction caused by blast exposure.

Use of the FE model of the entire chinchilla ear to simulate acoustic sound transmission from ear canal to cochlea may benefit from further validation. The middle ear pressure gain, cochlear impedance, and pressures in the cochlea should be calculated by the model and compared to experimental studies. In addition, refinement of the longitudinal BM displacement pattern predicted by the model may be pursued.

Improvement of the FE model for blast wave transmission is necessary in order for the model to provide accurate predictions. Notably, the application of the pressure input may need to be adjusted. In the analysis presented herein, the ear canal domain was initialized at rest (0 Pa and 0 m/s). While the pressure-inlet of the canal applied pressure and velocity to the system, there was zero momentum. Thus, modification of the ear canal domain so that the ear canal can be initialized with velocity may be a desirable modification to improve the model. An alternative method may instead apply the P0 pressure input closer to the TM. These modifications may improve the model. In addition to improving the model, experimental studies to determine the chinchilla TM and stapes displacement in response to blast exposure would be useful for validation. Measurement of the cochlea pressure and basilar membrane displacement in response to BOP would also facilitate validation.

References

ANSYS Inc. (2007). *Elements Reference*. SAS IP, Inc.

ANSYS Inc. (2009). Theory Reference for the Mechanical APDL and Mechanical Applications. In *Release 12.0* (Issue April). SAS.

ANSYS Inc. (2013). ANSYS Mechanical APDL Element Reference. In *Release 15.0*. SAS IP, Inc.

Arnold, S. (2000). The auditory brainstem response. In *Audiology: Diagnosis I* (pp. 451–470).

Békésy, G. Von. (1960). *Experiments in hearing*. McGraw-Hill.

Benefits Administration - The Office of Performance Analysis, V. (2019). *The Fiscal Year 2018 Annual Benefits Report*.

Chen, T., Smith, K., Jiang, S., Zhang, T., & Gan, R. Z. (2019). Progressive hearing damage after exposure to repeated low-intensity blasts in chinchillas. *Hearing Research*, *378*, 33–42. https://doi.org/10.1016/j.heares.2019.01.010

Cho, S. Il, Gao, S. S., Xia, A., Wang, R., Salles, F. T., Raphael, P. D., Abaya, H., Wachtel, J., Baek, J., Jacobs, D., Rasband, M. N., & Oghalai, J. S. (2013). Mechanisms of Hearing Loss after Blast Injury to the Ear. *PLoS ONE*, *8*(7). https://doi.org/10.1371/journal.pone.0067618

Daniel, S. J., Duval, M., Sahmkow, S., & Akache, F. (2007). Ototoxicity of topical moxifloxacin in a chinchilla animal model. *Laryngoscope*, *117*(12), 2201–2205. https://doi.org/10.1097/MLG.0b013e318148b275

DeKosky, S. T., Ikonomovic, M. D., & Gandy, S. (2010). Traumatic Brain Injury — Football, Warfare, and Long-Term Effects. *New England Journal of Medicine*,

363(14), 1293–1296. https://doi.org/10.1056/NEJMp1007051

DePalma, R. G., & Hoffman, S. W. (2018). Combat blast related traumatic brain injury (TBI): Decade of recognition; promise of progress. *Behavioural Brain Research*, *340*, 102–105. https://doi.org/10.1016/j.bbr.2016.08.036

Eldredge, D. H., Miller, J. D., & Bohne, B. A. (1981). A frequency-position map for the chinchilla cochlea. *Citation: The Journal of the Acoustical Society of America*, *69*, 1091. https://doi.org/10.1121/1.385688

Emadi, G., Richter, C.-P., & Dallos, P. (2004). Stiffness of the Gerbil Basilar Membrane: Radial and Longitudinal Variations. *Journal of Neurophysiology*, *91*(1), 474–488. https://doi.org/10.1152/jn.00446.2003

Engles, W. G., Wang, X., & Gan, R. Z. (2017). Dynamic Properties of Human Tympanic Membrane After Exposure to Blast Waves. *Annals of Biomedical Engineering*, *45*(10), 2383–2394. https://doi.org/10.1007/s10439-017-1870-0

Fausti, S. A., Wilmington, D. J., Gallun, F. J., Myers, P. J., & Henry, J. A. (2009). *Auditory and vestibular dysfunction associated with blast-related traumatic brain injury*. *46*(6), 797–810. https://doi.org/10.1682/JRRD.2008.09.0118

Gan, R. Z., Cheng, T., Dai, C., Yang, F., & Wood, M. W. (2009). Finite element modeling of sound transmission with perforations of tympanic membrane. *The Journal of the Acoustical Society of America*, *126*(1), 243–253. https://doi.org/10.1121/1.3129129

Gan, R. Z., Dai, C., Wang, X., Nakmali, D., & Wood, M. W. (2010). A totally implantable hearing system - Design and function characterization in 3D computational model and temporal bones. *Hearing Research*, *263*(1–2), 138–144.

https://doi.org/10.1016/j.heares.2009.09.003

Gan, R. Z., Feng, B., & Sun, Q. (2004). Three-dimensional finite element modeling of human ear for sound transmission. *Annals of Biomedical Engineering*, *32*(6), 847–859. https://doi.org/10.1023/B:ABME.0000030260.22737.53

Gan, R. Z., Nakmali, D., Ji, X. D., Leckness, K., Yokell, Z., & of Biomedical Engineering, P. (2016). Mechanical Damage of Tympanic Membrane in Relation to Impulse Pressure Waveform-A Study in Chinchillas HHS Public Access. *Hear Res*, *340*, 25–34. https://doi.org/10.1016/j.heares.2016.01.004

Gan, R. Z., Reeves, B. P., & Wang, X. (2007). Modeling of sound transmission from ear canal to cochlea. *Annals of Biomedical Engineering*, *35*(12), 2180–2195. https://doi.org/10.1007/s10439-007-9366-y

Greenwood, D. D. (1990). A cochlear frequency-position function for several species—29 years later. *The Journal of the Acoustical Society of America*, *87*(6), 2592–2605. https://doi.org/10.1121/1.399052

Guan, X., Chen, Y., & Gan, R. Z. (2014). Factors affecting loss of tympanic membrane mobility in acute otitis media model of chinchilla. *Hearing Research*, *309*(1), 136–146. https://doi.org/10.1016/j.heares.2013.12.005

Hall, D. A. (2012). fMRI of the central auditory system. In *Functional Neuroradiology: Principles and Clinical Applications* (pp. 575–591). Springer US. https://doi.org/10.1007/978-1-4419-0345-7_29

Hamernik, R. P., Turrentine, G., Roberto, M., Salvi, R., & Henderson, D. (1984). Anatomical correlates of impulse noise-induced mechanical damage in the cochlea. *Hearing Research*, *13*(3), 229–247. https://doi.org/10.1016/0378-5955(84)90077-7

Hickman, T. T., Smalt, C., Bobrow, J., Quatieri, T., & Liberman, M. C. (2018). Blast-induced cochlear synaptopathy in chinchillas. *Scientific Reports*, *8*(1), 1–12. https://doi.org/10.1038/s41598-018-28924-7

Hirsch, F. G. (1968). EFFECTS OF OVERPRESSURE ON THE EAR-A REVIEW. *Annals of the New York Academy of Sciences*, *152*(1), 147–162. https://doi.org/10.1111/j.1749-6632.1968.tb11972.x

Jiang, S., Smith, K., & Gan, R. Z. (2019). Dual-laser measurement and finite element modeling of human tympanic membrane motion under blast exposure. *Hearing Research*, *378*, 43–52. https://doi.org/10.1016/j.heares.2018.12.003

Le Prell, C. G., Hammill, T. L., & Murphy, W. J. (2019). Noise-induced hearing loss: Translating risk from animal models to real-world environments. *The Journal of the Acoustical Society of America*, *146*(5), 3646–3651. https://doi.org/10.1121/1.5133385

Leckness, K. (2016). *Novel Finite Element Method to Predict Blast Wave Transmission Through Human Ear* [University of Oklahoma]. https://hdl.handle.net/11244/44932

Leckness, K., Nakmali, D., & Gan, R. Z. (2018). Computational Modeling of Blast Wave Transmission Through Human Ear. *Military Medicine*, *183*, 262–268. https://doi.org/10.1093/milmed/usx226

Liberman, M. C., & Kujawa, S. G. (2017). Cochlear synaptopathy in acquired sensorineural hearing loss: Manifestations and mechanisms. In *Hearing Research* (Vol. 349, pp. 138–147). Elsevier B.V. https://doi.org/10.1016/j.heares.2017.01.003

Ouyang, J., Pace, E., Lepczyk, L., Kaufman, M., Zhang, J., Perrine, S. A., & Zhang, J. (2017). Blast-Induced Tinnitus and Elevated Central Auditory and Limbic Activity

in Rats: A Manganese-Enhanced MRI and Behavioral Study. *Scientific Reports*, *7*(1). https://doi.org/10.1038/s41598-017-04941-w

Patterson, J. H., & Hamernik, R. P. (1997). Blast overpressure induced structural and functional changes in the auditory system. *Toxicology*, *121*(1), 29–40. https://doi.org/10.1016/S0300-483X(97)03653-6

Peake, W. T., Rosowski, J. J., & Lynch, T. J. (1992). Middle-ear transmission: Acoustic versus ossicular coupling in cat and human. *Hearing Research*. https://doi.org/10.1016/0378-5955(92)90155-G

Race, N., Lai, J., Shi, R., & Bartlett, E. L. (2017). Differences in postinjury auditory system pathophysiology after mild blast and nonblast acute acoustic trauma. *Journal of Neurophysiology*, *118*(2), 782–799. https://doi.org/10.1152/jn.00710.2016

Ren, T., He, W., & Gillespie, P. G. (2011). *measurement of cochlear power gain in the sensitive gerbil ear*. https://doi.org/10.1038/ncomms1226

Rhode, W. S. (2007). Basilar membrane mechanics in the 6–9kHz region of sensitive chinchilla cochleae. *The Journal of the Acoustical Society of America*, *121*(5), 2792–2804. https://doi.org/10.1121/1.2718397

Ruggero, M. A., Rich, N. C., Robles, L., & Shivapuja, B. G. (1990). Middle-ear response in the chinchilla and its relationship to mechanics at the base of the cochlea. *The Journal of the Acoustical Society of America*, *87*(4), 1612–1629. https://doi.org/10.1121/1.399409

Smith, K. D., Chen, T., Rong, ;, & Gan, Z. (2020). Hearing Damage Induced by Blast Overpressure at Mild TBI Level in a Chinchilla Model. *MILITARY MEDICINE*, *185*, 2020. https://doi.org/10.1093/milmed/usz309

Song, H., Konan, L. M., Cui, J., Johnson, C. E., Langenderfer, M., Grant, D. A., Ndam, T., Simonyi, A., White, T., Demirci, U., Mott, D. R., Schwer, D., Hubler, G. K., Cernak, I., DePalma, R. G., & Gu, Z. (2018). Ultrastructural brain abnormalities and associated behavioral changes in mice after low-intensity blast exposure. *Behavioural Brain Research*, *347*, 148–157. https://doi.org/10.1016/j.bbr.2018.03.007

Stuhmiller, J. H., Phillips, Y. Y., & Richmond, D. R. (1991). Chapter THE PHYSICS AND MECHANISMS OF PRIMARY BLAST INJURY. In *Conventional Warfare: Ballistic, Blast, and Burn Injuries* (pp. 241–270). Office of the Surgeon General: Departement of the Army, United States of America.

Teudt, I. U., & Richter, C. P. (2014). Basilar membrane and tectorial membrane stiffness in the CBA/CaJ mouse. *JARO - Journal of the Association for Research in Otolaryngology*, *15*(5), 675–694. https://doi.org/10.1007/s10162-014-0463-y

Torre, P., & Fowler, C. G. (2000). Age-related changes in auditory function of rhesus monkeys (Macaca mulatta). *Hearing Research*, *142*(1–2), 131–140. https://doi.org/10.1016/S0378-5955(00)00025-3

Trevino, M., Lobarinas, E., Maulden, A. C., & Heinz, M. G. (2019). The chinchilla animal model for hearing science and noise-induced hearing loss. *The Journal of the Acoustical Society of America*, *146*(5), 3710–3732. https://doi.org/10.1121/1.5132950

Voss, S. E., Rosowski, J. J., & Peake, W. T. (2007). Non-ossicular signal transmission in human middle ears: Experimental assessment of the “acoustic route” with perforated tympanic membranes NIH Public Access. *J Acoust Soc Am*, *122*(4), 2135–2153.

https://doi.org/10.1121/1.2769617

Wang, X., & Gan, R. Z. (2016). 3D finite element model of the chinchilla ear for characterizing middle ear functions. *Biomechanics and Modeling in Mechanobiology*, *15*(5), 1263–1277. https://doi.org/10.1007/s10237-016-0758-5

Zhang, X., & Gan, R. Z. (2013). Finite element modeling of energy absorbance in normal and disordered human ears. *Hearing Research*, *301*, 146–155. https://doi.org/10.1016/j.heares.2012.12.005

Zhong, Z., Henry, K. S., Heinz, M. G., & Heinz, M. G. (2014). Sensorineural hearing loss amplifies neural coding of envelope information in the central auditory system of chinchillas. *Hear Res*, *309*, 55–62. https://doi.org/10.1016/j.heares.2013.11.006

Appendix A: List of Abbreviations

APDL	ANSYS Parametric Design Language
ABR	Auditory brainstem response
BM	Basilar membrane
BOP	Blast overpressure
CAS	Central auditory system
DPOAE	Distortion product otoacoustic emissions
FE	Finite element
FEM	Finite element method
FSIs	Fluid-structure interfaces or interactions
GUI	Graphical user interface
HPDs	Hearing protection devices
IACUC	Institutional Animal Care & Use Committee
μCT	Micro-computed tomography
MLR	Middle latency response
MOBs	Military occupational blasts
NIH	National Institutes of Health
PAS	Peripheral auditory system
PISO	Pressure-Implicit with Splitting of Operators
SC	Service-connected
SIMPLEC	SIMPLE-Consistent
SPL	Sound pressure level
Stapes FP	Stapes footplate

TM	Tympanic membrane
USDA	U.S. Department of Agriculture